

1  
2  
3  
4  
5  
6  
7  
8  
9  
10  
11  
12  
13  
14  
15  
16  
17  
18  
19  
20  
21  
22  
23  
24  
25  
26  
27  
28  
29  
30  
31  
32  
33  
34  
35  
36  
37  
38  
39  
40  
41  
42  
43  
44  
45  
46  
47  
48  
49  
50  
51

## **A cellular census of healthy lung and asthmatic airway wall identifies novel cell states in health and disease**

Vieira Braga, F.A.<sup>1,11\*</sup>, Kar, G.<sup>1,11\*</sup>, Berg, M.<sup>2,3,\*</sup>, Carpaij, O.A.<sup>3,4,§</sup>, Polanski, K.<sup>1,§</sup>, Simon, L.M.<sup>5</sup>, Brouwer, S.<sup>2,3</sup>, Gomes, T.<sup>1</sup>, Hesse, L.<sup>2,3</sup>, Jiang, J.<sup>2,3</sup>, Fasouli, E.S.<sup>1,11</sup>, Efremova, M.<sup>1</sup>, Vento-Tormo, R.<sup>1</sup>, Affleck, K.<sup>7</sup>, Palit, S.<sup>5</sup>, Strzelecka, P.<sup>1,13,14</sup>, Firth, H.V.<sup>1</sup>, Mahbubani, K.T.A.<sup>6</sup>, Cvejic, A.<sup>1,13,14</sup>, Meyer K.B.<sup>1</sup>, Saeb-Parsy, K.<sup>6</sup>, Luinge, M.<sup>2,3</sup>, Brandsma, C.-A.<sup>2,3</sup>, Timens, W.<sup>2,3</sup>, Angelidis, I.<sup>9</sup>, Strunz, M.<sup>9</sup>, Koppelman, G.H.<sup>3,10</sup>, van Oosterhout, A.J.<sup>7</sup>, Schiller, H.B.<sup>9</sup>, Theis, F.J.<sup>5,8</sup>, van den Berge, M.<sup>3,4</sup>, Nawijn, M.C.<sup>2,3,#,+</sup> & Teichmann, S.A.<sup>1,11,12,#,+</sup>

1. Wellcome Sanger Institute, Wellcome Genome Campus, Hinxton, Cambridge, CB10 1SA, United Kingdom.

2. University of Groningen, University Medical Center Groningen, Department of Pathology & Medical Biology, Groningen, The Netherlands. University of Groningen,

3. Groningen Research Institute for Asthma and COPD (GRIAC), University of Groningen, Groningen, The Netherlands.

4. University Medical Center Groningen, Department of Pulmonology, Groningen, The Netherlands

5. Helmholtz Zentrum München, German Research Center for Environmental Health, Institute of Computational Biology, Neuherberg, Germany.

6. Department of Surgery, University of Cambridge, and NIHR Cambridge Biomedical Research Centre, Cambridge, United Kingdom.

7. Allergic Inflammation Discovery Performance Unit, Respiratory Therapy Area, GlaxoSmithKline, Stevenage, United Kingdom.

8. Department of Mathematics, Technische Universität München, Munich, Germany.

9. Helmholtz Zentrum München, German Research Center for Environmental Health, Institute of Lung Biology and Disease, Group Systems Medicine of Chronic Lung Disease, and Translational Lung Research and CPC-M bioArchive, Member of the German Center for Lung Research (DZL), Munich, Germany.

10. University of Groningen, University Medical Center Groningen, Department of Pediatric Pulmonology and Pediatric Allergology, Beatrix Children's Hospital, Groningen, The Netherlands.

11. Open Targets, Wellcome Genome Campus, Hinxton, Cambridge CB10 1SA, United Kingdom.

12. Theory of Condensed Matter Group, Cavendish Laboratory/Dept Physics, University of Cambridge, JJ Thomson Avenue, Cambridge CB3 0EH, UK

13. Department of Haematology, University of Cambridge, Cambridge, CB2 0XY, UK

14. Cambridge Stem Cell Institute, Cambridge CB2 1QR, UK

\* These authors contributed equally to this work.

§ These authors contributed equally to this work.

# These authors share senior authorship.

+To whom correspondence should be addressed: m.c.nawijn@umcg.nl, st9@sanger.ac.uk

52 **Summary**

53 Human lungs enable efficient gas exchange, and form an interface with the environment  
54 which depends on mucosal immunity for protection against infectious agents. Tightly  
55 controlled interactions between structural and immune cells are required to maintain lung  
56 homeostasis. Here, we use single cell transcriptomics to chart the cellular landscape of  
57 upper and lower airways and lung parenchyma in health. We report location-dependent  
58 airway epithelial cell states, and a novel subset of tissue-resident memory T cells. In lower  
59 airways of asthma patients, mucous cell hyperplasia is shown to stem from a novel mucous  
60 ciliated cell state, as well as goblet cell hyperplasia. We report presence of pathogenic  
61 effector Th2 cells in asthma, and find evidence for type-2 cytokines in maintaining the altered  
62 epithelial cell states. Unbiased analysis of cell-cell interactions identify a shift from airway  
63 structural cell communication in health to a Th2-dominated interactome in asthma.

64

65

66

## 67 Introduction

68 The lung plays a critical role in both gas exchange and mucosal immunity, and its anatomy  
69 serves these functions through (1) the airways that lead air to the respiratory unit, provide  
70 mucociliary clearance, and form a barrier against inhaled particles and pathogens; and (2)  
71 the alveoli, distal saccular structures where gas exchange occurs. Acute and chronic  
72 disorders of the lung are a major cause of morbidity and mortality worldwide<sup>1</sup>. To better  
73 understand pathogenesis of lung disease, it is imperative to characterise the cell types of  
74 the lung and understand their interactions in health<sup>2,3</sup> and disease. The recent identification  
75 of the ionocyte as a novel airway epithelial cell-type<sup>4,5</sup> underscores our incomplete  
76 understanding of the cellular landscape of the lung, which limits our insight into the  
77 mechanisms of respiratory disease, and hence our ability to design therapies for most lung  
78 disorders.

79  
80 We set out to profile lung-resident structural and inflammatory cells and their interactions by  
81 analysing healthy human respiratory tissue from four sources: nasal brushes, endobronchial  
82 biopsies and brushes from living donors, and tissue samples from lung resections and  
83 transplant donor lungs. Our single cell analysis identifies differences in the proportions and  
84 transcriptional phenotype of structural and inflammatory cells between upper and lower  
85 airways and lung parenchyma. Using an unbiased approach to identify tissue-resident CD4  
86 T cells in airway wall, we identify a novel tissue migratory CD4 T cell (TMC) that harbours  
87 features of both circulating memory cells and of tissue resident memory cells (TRM) CD4 T  
88 cells. We demonstrate that many disease-associated genes have highly cell type-specific  
89 expression patterns. This holds true for both rare disease-associated genes, such as CFTR  
90 mutated in cystic fibrosis, as well as genes associated with a common disease such as  
91 asthma.

92  
93 In addition, we evaluate the altered cellular landscape of the airway wall in chronic  
94 inflammatory disease using bronchial biopsies from asthma patients. We identify a novel  
95 epithelial cell state highly enriched in asthma, the mucous ciliated cell. Mucous ciliated cells  
96 represent a transitioning state of ciliated cells with molecular features of mucus production,  
97 and contribute to mucous cell hyperplasia in this chronic disease. Other changes associated  
98 with asthma include increased numbers of goblet cells, intraepithelial mast cells and  
99 pathogenic effector Th2 cells in airway wall tissue. We examine intercellular communications  
100 occurring in the healthy and asthmatic airway wall, and reveal a remarkable loss of epithelial  
101 communication and a concomitant increase in Th2 cell interactions. The newly identified  
102 TMC subset interacts with epithelial cells, fibroblasts and airway smooth muscle cells in  
103 asthma. Collectively, these data generate novel insights into epithelial cell changes and  
104 altered communication patterns between immune and structural cells of the airways, that  
105 underlie asthmatic airway inflammation.

## 106 **A human lung cell census identifies macro-anatomical patterns of epithelial cell** 107 **states across the human the respiratory tree**

108 The cellular landscape along the 23 generations of the airways in human lung is expected  
109 to differ both in terms of relative frequencies of cell types and their molecular phenotype<sup>6</sup>.  
110 We used 10x Genomics Chromium droplet single-cell RNA sequencing (scRNA-Seq) to  
111 profile a total of 36,931 single cells from upper and lower airways, and lung parenchyma  
112 (Figure 1A, B). We profiled nasal brushes, and (bronchoscopic) brushes and biopsies from  
113 airway wall (third to sixth generation) from healthy volunteers. For parenchyma (small  
114 respiratory airways and alveoli), we obtained lung tissue from deceased transplant donors,  
115 also analysed on the 10x platform, and from non-tumour resection tissue from lung cancer

116 patients, analysed on a bespoke droplet microfluidics platform based on the Dropseq  
117 protocol<sup>7</sup>.

118  
119 Integration of the data from nasal epithelium, airway wall and parenchymal tissue reveals a  
120 diversity of epithelial, endothelial, stromal and immune cells, with approximately 21 coarse-  
121 grained cell types in total (Figures 1 and 2, Extended Figure 1), that can be explored in user-  
122 friendly web portal ([www.lungcellatlas.org](http://www.lungcellatlas.org)). Analysis of parenchymal lung tissue from  
123 resection material using Dropseq led to the identification of 15 coarse-grained cell  
124 populations (epithelial and non-epithelial) (Extended Figure 2). Using MatchScore<sup>8</sup> to  
125 quantify the overlap between cell type marker signatures between the two datasets revealed  
126 an extensive degree of overlap in cell type identities (Extended Figure 2). In our analysis  
127 below, we first concentrate on epithelial cells (Figure 1), and then focus on the stromal and  
128 immune compartments (Figure 2).

129  
130 In the epithelial lineage, we identified a total of at least 10 cell types across the upper and  
131 lower airways and lung parenchyma (Figure 1C, Extended Data Figure 1). We detected  
132 multiple basal, club, ciliated and goblet cell states, as well as type-1 (T1) and type-2 (T2)  
133 alveolar cells, and the recently described ionocyte<sup>4,5</sup> (Extended Figure 3). Both goblet and  
134 ciliated cells were present in the nasal epithelium (Figure 1D). In the lower airways, we  
135 detected basal, club and ciliated cells as well as ionocytes, but only very small numbers of  
136 goblet cells. T1 and T2 cells were, as expected, only found in the lung parenchyma (Figure  
137 1E).

138  
139 We did not identify specific clusters of tuft cells or neuroendocrine (NE) cells. Since cell  
140 types represented by a small fraction of the data might be missed by unsupervised  
141 clustering, we evaluated the expression of known marker genes for NE cells (CHGA,  
142 ASCL1, INSM1, HOXB5) and Tuft cells (DCLK1, ASCL2)<sup>4</sup>. NE marker genes identified a  
143 small number of cells, present only in lower airways, displaying a transcriptional profile  
144 consistent with that of NE cells (extended Figure 4). Tuft cell marker genes did not identify  
145 a unique cell population. Ionocytes were found in lower airways, and at very low frequency  
146 in upper airways, but were completely absent from the parenchyma. Comparison of the cell  
147 populations identified using the two different bronchoscopic sampling methods (brush  
148 versus biopsy) in lower airways showed that basal cells were captured most effectively in  
149 biopsies, while apical epithelial cells, such as ciliated and club cells were relatively  
150 overrepresented in the bronchial brushings (Figure 1D).

151  
152 Our dataset allowed us to identify two discrete cell states in basal, goblet and ciliated  
153 epithelial cells. Some of these cell phenotypes were restricted to specific anatomical  
154 locations along the respiratory tract. Basal cells were present in both upper and lower  
155 airways, although at relatively low frequency in upper airways (Figure 1E). The two basal  
156 cell states corresponded to differentiation stages, with the less mature Basal 1 cell state  
157 expressing higher levels of *TP63* and *NPPC* in comparison to Basal 2 cells (Figure 1F and  
158 extended data 1), which were more abundant in bronchial brushes, suggesting a more apical  
159 localization for these more differentiated basal cells (Figure 1D). Goblet 1 and 2 cells were  
160 both characterized by high expression of *CEACAM5*, *S100A4*, *MUC5AC* and lack of *MUC5B*  
161 (Figure 1F and Extended Figures 1 and 4). Goblet 1 cells specifically express *KRT4* and  
162 *CD36* (Figure 1G and Extended Figure 4). Genes involved with immune function, such as  
163 *IDO1*, *NOS2*, *IL19*, *CSF3* (Granulocyte-colony stimulating factor) and *CXCL10* are  
164 expressed at high levels in Goblet 2 cells (Figure 1G and Extended Figure 4). These  
165 molecules enriched in Goblet 2 cells are involved in recruitment of neutrophils, monocytes,  
166 dendritic cells and T cells<sup>9</sup>. Both goblet cells states are present in upper airway epithelium,

167 with Goblet 1 cells being more frequent. In contrast, the Goblet 2 cell state was also present  
168 in lower airways, albeit at low abundance (Figure 1E).

169  
170 Ciliated cell transcriptional phenotypes are also zoned in terms of their presence across  
171 macro-anatomical locations, with a discrete ciliated cell state more abundant in upper  
172 airways (Ciliated 2) compared to lower airways and parenchyma. Nasal epithelial Ciliated 2  
173 cells express pro-inflammatory genes, such as *CCL20* (Extended data 3) and higher levels  
174 of metabolic genes (*ATP12A* and *COX7A1*) and vesicle transport (*AP2B1* and *SYT5<sup>10</sup>*)  
175 compared to the Ciliated 1 cell state. In contrast, the Ciliated 1 cells from lower airways  
176 specifically expressed genes involved in cytoprotection (*PROS1<sup>11</sup>*) and fluid reabsorption  
177 (*FXYD1<sup>12</sup>*) (Figure 1H and Extended Figure 4). Interestingly, comparison of the location-  
178 specific differences between ciliated and goblet cells identified a transcriptional signature  
179 specific for the upper airways present in both epithelial cell types (Extended Figure 4B).

180  
181 Next, we assessed the contribution of specific epithelial cell types to Mendelian disease.  
182 Cell-type specific expression patterns of genes associated with Mendelian disorders (based  
183 on the Online Mendelian Inheritance in Man, OMIM database) confirm ionocytes as  
184 particularly high expressers of the *CFTR* gene, mutated in cystic fibrosis (Figure 1I). These  
185 cells also express *SCNN1B*, mutations of which can cause bronchiectasis, another feature  
186 of cystic fibrosis, suggesting a potential key pathological role for ionocytes in both  
187 bronchiectasis and cystic fibrosis. In addition, expression of *SERPINA1* (Figure 1I) was  
188 found to be enriched in type-2 alveolar epithelial cells, underscoring their role in alpha-1-  
189 antitrypsin deficiency<sup>13</sup>.

## 190 **Differential anatomical distribution of the stromal and immune components in the** 191 **human respiratory tree**

192 Next, we analysed the single cell transcriptomes of immune and stromal cells from the upper  
193 airways, lower airways and the lung parenchyma (Figure 2A). We identified immune clusters  
194 of myeloid (macrophages, neutrophils, dendritic cells (DCs) and mast cells) and lymphoid  
195 cells (T and NK cells, B cells; Figure 2B, and Extended Figure 5). Immune and stromal cell  
196 numbers and composition varied greatly across different anatomical regions (Figure 2A and  
197 2C). Nasal brushes contained only a small number of immune cells, with the large majority  
198 being dendritic cells. In the lower airways, the fraction of inflammatory cells was significantly  
199 larger and relatively enriched for macrophages (Figure 2C and Extended Figure 5), which  
200 was directly confirmed by cell composition comparison of upper *versus* lower airway brushes  
201 obtained from the same donor (Extended Figure 5E).

202  
203 Macrophages show large donor variation in their phenotype (Extended figure 5), but they all  
204 share high expression of *MARCO*, *CCL18* and genes involved in apolipoprotein metabolism  
205 (*APOC1* and *APOE*) (Figure 2E). Lung neutrophils express high levels of the granulocyte  
206 markers *S100A8*, *S100A12<sup>14</sup>* and *LILRA5*, a receptor poorly characterised in the lungs, that  
207 has been shown to have a proinflammatory function in synovial fluid macrophages<sup>15</sup> (Figure  
208 2E). DCs were mostly myeloid, with high expression of *CD1E*, *CD1C*, *CLEC10A* (Figure 2E)  
209 and of *FCER1A* (IgE receptor) and *CCL17*, molecules known to play a key role in  
210 inflammatory conditions such as asthma<sup>16</sup>.

211  
212 In the droplet RNAseq data sets, we could not distinguish CD4+ and CD8+ T cells and NK  
213 cells from each other (Figure 2B). The B cells in our dataset were mostly plasma cells,  
214 expressing high levels of *JCHAIN* (Joining Chain of Multimeric IgA And IgM). IgM+ (*IGHM*)  
215 cells were enriched in the airway lumen and in the lung parenchyma, while IgG3+ (*IGHG3*)  
216 were enriched in airway biopsy samples and were virtually absent from the airway lumen.



217 This suggests an isotype-driven micro-anatomical segregation of B cells in the airways  
218 (Extended Figure 5F).

## 219 **Molecular features of mucous cell metaplasia in asthma**

220 To characterize the changes in the cellular landscape of airway wall in a chronic  
221 inflammatory condition, we also analysed bronchial biopsies from six volunteers with  
222 persistent, childhood-onset asthma (Figure 3A). Asthma is a complex disease<sup>17</sup> and multiple  
223 cells such as epithelial<sup>18,19</sup>, endothelial<sup>20</sup> and immune cells<sup>21,22</sup> have been shown to be  
224 altered in asthma. The combined airway wall dataset reveals a cellular landscape dominated  
225 by epithelial (*EPCAM*-positive) cells, with minor contributions from endothelial,  
226 mesenchymal and immune cells (Extended Figure 6A and B).

227  
228 High-resolution clustering of the *EPCAM*<sup>+</sup> clusters identifies 10 sub clusters representing the  
229 6 epithelial cell types observed in healthy airway wall (Figure 1C), as well as two additional  
230 basal cell states: a mucous ciliated cell state, and serous cells from the submucosal glands  
231 (Figure 3B). In addition to the two basal cell states observed in healthy airway wall (Figure  
232 1C), the basal cell states in asthma include activated and cycling cell states (Figure 3B).  
233 Activated basal cells closely resemble Basal 1 cells in their transcriptional phenotype, but  
234 also express proinflammatory genes such as *POSTN* (Figure 3D). Cycling basal cells are  
235 characterized by expression of canonical marker genes of proliferating cells (*MKI67* and  
236 *TOP2A*) (Figure 3D), and this is the only cluster of airway epithelial cells expressing the  
237 squamous cell marker *KRT13* (Extended Figure 6).

238  
239 We observe mucous cell hyperplasia in asthma, with a strong increase in goblet cell  
240 numbers (Figure 3C), which are very rare in healthy airway wall biopsies (Figure 1E).  
241 Moreover, the goblet cell transcriptional phenotype is altered in asthma, with strongly  
242 increased expression of *MUC5AC* and *SPDEF*, as well as proinflammatory and remodelling  
243 genes including *NOS2*, *CEACAM5* and *CST1* (Figure 3D). In addition, we identify a strong  
244 increase in mucous ciliated cells, a novel cell state that has remarkable transcriptional  
245 resemblance to ciliated cells, whilst co-expressing a number of mucous genes, including  
246 *MUC5AC*, *SERPINB2/3* and *CEACAM5* (Figure 3D, Extended Figure 6). Mucous ciliated  
247 cells lack expression of the transcription factor *SPDEF* (in contrast to club and goblet cells),  
248 while maintaining *FOXJ1* expression, underscoring their ciliated cell origin (Extended Figure  
249 7).

250  
251 To further dissect the inferred differentiation trajectories in healthy and asthmatic airway wall  
252 epithelial cells, we performed pseudotime analysis<sup>23</sup>. This reveals a trajectory starting with  
253 basal cell subsets, bifurcating into either a secretory lineage (mainly club cells) or a ciliated  
254 lineage in healthy airway wall (Figure 3E). In asthma, the secretory lineage is a mix of club  
255 and goblet cells, while the mucous ciliated cell state overlaps with the ciliated differentiation  
256 trajectory (Figure 3E,F).

257  
258 Next, we further analysed the transcriptional profiles of the two mucous cell states we  
259 observe specifically in asthma: the mucous ciliated cells and the goblet cells. As both  
260 NOTCH and IL4/IL13 signalling have been shown to contribute to mucous cell  
261 differentiation<sup>24</sup>, we analysed expression of both NOTCH target genes<sup>25,26</sup> and IL4/IL13  
262 target genes<sup>27</sup> in club, goblet, and ciliated cells as well as in the novel mucous ciliated cell  
263 state, in both asthma and healthy airway wall biopsies. Expression of IL4/IL13-induced  
264 genes<sup>27</sup> is prominent in asthma, and highest in activated basal cells, goblet cells and mucous  
265 ciliated cells (Extended Figure 7). In club cells, expression of NOTCH target genes<sup>25,26</sup> is  
266 not different between asthma and healthy-derived cells. In contrast, in goblet cells, the

267 NOTCH target gene signature is retained only in cells from healthy airway wall, and is lost  
268 in asthma.

269  
270 As in goblet cells, mucous ciliated cells also lack expression of Notch target genes in asthma  
271 (Extended Figure 7). Hence, we postulate that mucous ciliated cells represent a transition  
272 cell state in the ciliated lineage - induced by IL4/IL13 signalling - leading to a mucous cell  
273 phenotype which contributes to mucous cell metaplasia in asthma<sup>24</sup>. Similar to goblet cells,  
274 mucous ciliated cells express asthma genes such as *CST1*<sup>28</sup> and *POSTN* (Figure 3D),  
275 indicating that these cells also contribute to airway inflammation and remodelling.

276  
277 Integrating the asthma GWAS genes with our epithelial single cell transcriptomic data  
278 reveals a broad contribution of the airway epithelial cell types to asthma susceptibility (Figure  
279 3G), with high expression of asthma GWAS genes in ciliated and mucous ciliated cells. This  
280 includes genes involved in cilia function (*DYNC2H1* and *KIF3A*), cell adhesion (*ELK3*,  
281 *CDHR3* and *PTPRT*) and IL5-induced mucus metaplasia (*IL5RA*)<sup>29</sup>, further suggesting a  
282 direct link between mucous ciliated cells and Th2 CD4 T cells.

### 283 284 **Remodelling of the stromal and Immune compartments in asthmatic airways**

285 Asthma is associated with chronic inflammation and remodelling of the airway wall<sup>30</sup>.  
286 Analysis of the inflammatory and stromal cell populations in the bronchial biopsies by  
287 unsupervised clustering (Figure 4A) reveals the presence of B and T cells, neutrophils,  
288 macrophages, DCs, mast cells, fibroblasts, smooth muscle cells and endothelial cells  
289 (Figure 4B, Extended Figure 8). We did not detect any innate lymphoid cells, basophils or  
290 eosinophils as separate clusters (Extended Figure 8). Analysis of bulk transcriptome  
291 analysis of whole airway biopsies before and after tissue dissociation identified very low  
292 expression levels of eosinophil marker genes (*CLC* and *IL5RA*), indicating these cells are  
293 relatively rare in the samples we analysed (Extended Figure 9).

294  
295 Mast cell numbers were increased in asthma (Figure 4C), while being virtually absent in the  
296 airways of healthy individuals (Figure 4C). Mast cells in asthmatic airways lack chymase 1  
297 expression (*CMA1*) and express high levels of tryptase genes (*TPSB2*, *TPSAB1*) (Figure  
298 4D). Prostaglandins and leukotrienes are known to be crucial to inflammatory cell signalling.  
299 Mast cells express high levels of *PTGS2* and *HPGDS* (Figure 4D, Extended Figure 10).  
300 *PTGS2* (cyclooxygenase-2), also known as inflammatory cyclooxygenase, converts the  
301 precursor arachidonic acid to prostaglandin endoperoxide H<sub>2</sub> (PGH<sub>2</sub>). *HPGDS*  
302 (Hematopoietic Prostaglandin D Synthase) catalyses the conversion of PGH<sub>2</sub> to  
303 prostaglandin D<sub>2</sub> (PGD<sub>2</sub>). PGD<sub>2</sub> activates CD4 Th2 cells<sup>31</sup>, ILC2<sup>32</sup>, basophils and  
304 neutrophils<sup>31</sup> and plays a key role in asthma pathology. Expression of all PGD<sub>2</sub> biosynthesis  
305 enzymes is a unique feature of mast cells (Extended Figure 10) and this suggests that  
306 intraepithelial mast cells are continually producing PGD<sub>2</sub> in asthma patients. Thus, these  
307 cells are most likely intraepithelial mast cells, previously shown to accumulate in Th2-high  
308 asthmatic airway epithelium<sup>33</sup>, and reported to be increased<sup>34</sup> with disease severity<sup>21</sup>.

309  
310 We observed an increase in the number of B cells in the asthmatic airways ( Figure 4C) and  
311 these cells have a plasma cell phenotype, with high *JCHAIN* expression (Figure 4D). The  
312 increase in B cell numbers was mostly of IgM+ cells (*IGHM*) (Figure 4E). IgM levels in  
313 asthma BALF samples have been reported to be either increased<sup>34</sup> or unchanged<sup>35</sup>,  
314 suggesting cohort dependent variability. IgM-producing B cells in the healthy airways were  
315 mostly present in the airway lumen (Extended Figure 5F). However, as we did not analyse  
316 brush samples from asthmatic patients, we cannot precisely pinpoint whether the increase  
317 in IgM+ B cells takes place in the intraepithelial region or in the lumen, as both regions are  
318 present in biopsy samples.

319

320 Asthma GWAS genes show highly cell-type restricted expression (Figure 4F). When  
321 excluding the widely expressed HLA genes from the analysis, fibroblasts and T cells express  
322 the highest number of asthma GWAS genes (Figure 4F), which are mostly upregulated in  
323 asthma (Figure 4F). GATA3 expression is restricted to T cells (Figure 4F), and increased in  
324 T cells from asthma patients (Figure 4F and G). We detected increased expression of CD4  
325 (but not CD8a) in the T cell cluster, suggesting an increase in Th2 CD4 T cells (Figure 4G).  
326 Therefore, we next proceed to investigate the CD4 T cell compartment in depth.

### 327 **Pathogenic effector Th2 cells are enriched in asthmatic airways**

328 In line with the increase in GATA3 and CD4 expression mentioned above, CD4 Th2 cells  
329 are known to be key drivers of asthma<sup>17,36</sup>. To assess the presence of Th2 effector cells in  
330 the airways of asthma patients (Figure 4G), we single cell sorted CD4 T cells followed by  
331 plate-based SmartSeq2 analysis for in depth transcriptional phenotyping of the T helper cell  
332 compartment (see Methods for details). We analysed cells from both peripheral blood and  
333 airway wall biopsies (Figure 5A) from a larger cohort of asthma patients and healthy controls  
334 (Figure 5B). Unbiased clustering reveals six major populations of CD4 T cells (Figure 5C  
335 and Extended Figure 11). At this coarse level of analysis, none of these six clusters was  
336 specifically enriched in asthma patients (Figure 5D).

337  
338 Comparative analysis of CD4 T cells isolated from paired blood and lung samples allows us  
339 to differentiate between tissue-resident T cells and circulating T cells in an unbiased way,  
340 by subtracting the populations shared with blood from the populations specific to the  
341 biopsies (Figure 5E). Using this approach, we identified two subsets highly enriched in the  
342 lungs: the classical Tissue Resident Memory (TRM) CD4 T cells, and a novel subset we  
343 named Tissue Migratory CD4 T cell (TMC) (Figure 5E). Naive/central memory (CM), effector  
344 memory (EM), and EMRA cells, as well as a mixed Treg/Th2 cluster, are either enriched in  
345 blood or present in both blood and airways (Figure 5E).

346  
347 To better understand the two distinct lung-restricted CD4 T cell subsets, we performed  
348 differential expression analysis between TRM and TMC cells (Figure 5F). Several  
349 transcription factors highly expressed in circulating cells are enriched in TMC cells, such as  
350 *LEF1*, *SATB1* and *KLF3*, while *ZEB2* is specific for TRM cells. TMC cells expressed the  
351 tissue egression markers *S1PR1*, *CCR7* and *SELL* (CD62L) and lacked expression of the  
352 canonical TRM marker *ITGAE* (CD103) (Figure 5F). As low numbers of TMC cells were  
353 present in peripheral blood CD4 T cells (Figure 5E), these data suggest that these cells have  
354 the potential to transit between lung and blood, a hypothesis supported by pseudotime  
355 trajectory analysis of the CD4 T cell subsets (Extended Figure 12).

356  
357 Protein expression of CD69 and CD103 (ITGAE) have both been used as hallmarks of lung  
358 resident CD4 T cells isolated from lung parenchyma<sup>37,38</sup>, but to the best of our knowledge,  
359 no similar analysis of lung airway epithelial CD4 T cells has been performed to date. Both  
360 TMC and TRM cells have high expression of CD69, but only TRM cells express ITGAE  
361 (Extended Figure 11), suggesting these subsets might be equivalent to the previously  
362 described cells<sup>37,38</sup>. However, TRM cells<sup>37,38</sup> have been shown to lack S1PR1 and CCR7  
363 protein expression, in contrast to TMC cells that express high mRNA levels of both markers.  
364 No direct whole transcriptome comparison of CD69+CD103+ *versus* CD69+CD103- TRMs  
365 has been performed yet<sup>37,38</sup>. Further studies are necessary to properly compare CD4 T cells  
366 from airway wall *versus* lung parenchyma, and investigate how TMC align with the previously  
367 reported TRM subsets at the transcriptome level.

368



369 TRM cells in airway wall expressed high levels of *CXCR6* and *ITGA1* and high levels of  
370 cytokines (*CCL4*, *CCL4L2*, *CCL5*) and effector molecules (*PRF1*, *GZMB*, *GZMA*, *GZMH*)  
371 (Figure 5F and Extended Figure 11), indicating they are also in a primed state capable of  
372 direct effector function, as recently shown for TRMs from lung parenchyma<sup>37</sup>.

373  
374 CD4 effector T cells are classically divided into distinct functional subsets based on their  
375 cytokine profile<sup>17</sup>. We manually annotated clusters of Th1 (*IFNG*<sup>+</sup>), Th2 (*IL4*<sup>+</sup>, *IL5*<sup>+</sup> or *IL13*<sup>+</sup>)  
376 and Th17 (*IL17A*<sup>+</sup> or *IL17F*<sup>+</sup>) cells based on their cytokine expression profiles (Figure 5G,  
377 Extended Figure 13). Cytokine-producing cells were mostly retrieved from the biopsies, with  
378 only very few present in blood (Extended Figure 14).

379  
380 In terms of absolute numbers, Th2 cells were very rare and found both in healthy and  
381 asthmatic patients, although numbers of Th2 cells were significantly increased in the airway  
382 wall in the asthma patients, with no detected difference in the relative proportions of the  
383 other subsets (Figure 5H). In addition to the signature cytokines and the transcription factor  
384 *GATA3* (Extended Figure 13), airway wall Th2 cells express *HGPDS*, identifying them as  
385 pathogenic effector Th2 (peTh2) cells, previously associated with eosinophilic inflammation  
386 of the gastrointestinal tract and skin<sup>39</sup>. Airway Th2 also express the transcription factor  
387 *PPARG*, and cytokine receptors *IL17RB* and *IL1RL1* (Figure 5I). *IL17RB* and *IL1RL1* have  
388 been reported as upregulated in pathogenic allergen-specific Th2 cells (coined Th2A cells),  
389 which are present in allergic disease<sup>40</sup> as well as in chronic rhinosinusitis with nasal polyps<sup>41</sup>,  
390 suggesting airway wall Th2 cells share features with both Th2A and peTh2 cells.

### 391 **Asthma is characterized by specific signalling networks**

392 Asthma is characterized by remodelling of the airways, which depends on complex  
393 interactions between structural and inflammatory cells<sup>17</sup>, both *via* direct physical interactions  
394 and *via* secreted proteins and small molecules. We used our recently developed  
395 receptor/ligand database and statistical inference framework CellPhoneDB<sup>42</sup>  
396 ([www.cellphonedb.org](http://www.cellphonedb.org)), to chart combinatorial cell-specific expression patterns of genes  
397 encoding receptor/ligand pairs. We aim to identify potential cell-cell interactions in the airway  
398 wall, and define their changes in asthma. Whilst most interactions are unchanged, some  
399 were specific to the diseased or healthy state (Full list in Extended 6).

400  
401 In healthy controls, the cell-cell interaction landscape of the airway wall was dominated by  
402 lung structural cells (mainly mesenchymal and epithelial cell types) communicating with  
403 other lung structural cells and with tissue-resident T cells, both the classical TRM and the  
404 newly identified TMC subsets (Figure 6A,B, left panels). In the asthmatic airway wall, the  
405 number of predicted interactions between epithelial and mesenchymal cells was strongly  
406 reduced. Instead, the cell-cell communication landscape in asthmatic airway wall is  
407 dominated by Th2 cells that were found to have increased interactions with other immune  
408 cells, including antigen-presenting cells, and also with epithelial cells (Figure 6A,B, right  
409 panels). The most striking increase in interactions is with mesenchymal cells, both  
410 fibroblasts and smooth muscle cells (Figure 6A and B, right panels).

411  
412 Analysis of the predicted cell-cell interactions between structural cells in healthy airway wall  
413 revealed a wealth of growth factor-signalling pathways including the FGF, GFR, IGF, TGF,  
414 PDGF and VEGF pathways, most of which were lost in the asthmatic samples (Figure 6C).  
415 Detailed analysis of the individual interactions of Th2 cells with the inflammatory and lung  
416 structural cells unique to asthma revealed the potential of Th2 cells to have cognate  
417 interactions with the epithelial cells involving KLRG1 and CD103 binding to E-cadherin, and  
418 also integrin-mediated interactions with epithelial-expressed matrix proteins such as

419 Tenascin-C. Epithelial expression of alarmins and cytokines, such as IL33, TSLP (Figure  
420 3G) and TNFSF10/TRAIL (Figure 6D), all of which are asthma genes<sup>43-45</sup>, might then lead  
421 to activation of Th2 cells expressing the receptors.  
422

423 In addition to validating these well-known interactions, which for IL33 and TSLP failed to  
424 reach significance in our unbiased cell-cell interaction analysis, we identify novel epithelial-  
425 Th2 cell interactions in asthma, including chemokines CXCL2 and CXCL17, and the cytokine  
426 MIF that are all expressed by epithelial cells, while Th2 cells express the respective  
427 receptors (Figure 6C). Interestingly, mesenchymal cells share some of these Th2 cell  
428 interactions, such as expression of TNFSF10/TRAIL and MIF. Predicted Th2 interactions  
429 unique to mesenchymal cells in asthmatic airway wall are CXCL12 and CCL11, expressed  
430 by fibroblasts and smooth muscle cells. Airway wall Th2 cells in asthma express the  
431 cytokines IL5 and IL13 (Figure 5I), the receptor complexes for which are expressed by  
432 immune cells and epithelial cells, respectively, in line with the expression of IL13-driven  
433 genes in mucous ciliated and goblet cells in asthma (Extended data Figure 7). In addition to  
434 these classical Th2 cytokines, Th2 cells express LTB for which basal epithelial cells express  
435 the receptor.  
436

437  
438  
439  
440  
441

## 442 Discussion

443

444 Our study profiles the cellular landscape of human lung tissue at the single-cell level,  
445 including both upper and lower airways and parenchymal lung tissue in healthy adults. We  
446 identify at least 21 main cell types in the normal human lung, that can be further subdivided  
447 into more fine-grained cell states. There is clear Mendelian disease relevance for many cells,  
448 including the previously-reported ionocytes (for bronchiectasis and cystic fibrosis), and type-  
449 2 alveolar cells (for alpha-1-antitrypsin deficiency) . We chart differences in frequencies and  
450 molecular state of airway epithelial cells between upper and lower airways. To our  
451 knowledge, we provide for the first time a detailed molecular description of tissue-resident  
452 CD4 T cells in the human lower airway wall, and identify two separate subsets, one of which  
453 was hitherto unknown.

454

455 In our studies, we deployed two different droplet-based single-cell RNA sequencing  
456 platforms and one plate-based method, with experiments performed in three geographically  
457 distinct research centers. Overall, the datasets are remarkably consistent, which yields a  
458 quantitative dataset of the cellular composition of human upper and lower airways and lung  
459 parenchyma.

460

461 In addition to analysing healthy reference samples, we characterize the changes in the cell  
462 types and cell states in airway wall in asthma. This reveals mucous ciliated cells as a novel  
463 cell state that contributes to mucous cell metaplasia. Both mucous ciliated and goblet cells  
464 are characterized by expression of an IL4/IL13-driven gene signature, indicating a dominant  
465 role for type-2 cytokines in maintaining the epithelial changes in chronic airway inflammation  
466 in asthma. The mucin gene expression induced in FOXP1+ cells with an unabated ciliated  
467 cell transcriptional profile strongly indicates that the mucous state is superimposed on the  
468 ciliated cell phenotype, independent of goblet cell differentiation from club cells. Our data  
469 seem to indicate that these two processes can occur in parallel, with mucous metaplasia of  
470 ciliated cells and goblet cell hyperplasia both contributing to the increase in mucin-producing  
471 cells in asthma. Whether the mucous ciliated cells go on to lose their FOXP1 expression and  
472 the ciliated transcriptional profile and transdifferentiate into *bona fide* SPDEF-positive goblet  
473 cells remains to be firmly established.

474

475 The epithelial cell changes in airway wall in asthma are surprisingly different to those  
476 recently described in patients with in chronic rhinosinusitis with polyps<sup>27</sup>. In this chronic  
477 inflammatory disease of the upper airways caused by exaggerated type-2 immunity, an  
478 IL4/IL13-driven gene transcription profile was mainly observed in basal epithelial cells, which  
479 were found to be arrested in differentiation and highly increased in numbers<sup>27</sup>. Using the  
480 same IL4/IL13-driven gene module, we find some expression thereof in basal cells, but in  
481 asthma this does not result in significant changes in basal cell numbers. Instead, we observe  
482 an increased number of goblet cells, as well as of mucous ciliated cells, both of which show  
483 evidence of marked expression of the IL4/IL13-driven gene signature (extended data Figure  
484 7). Hence, while there is some overlap in the cellular mechanisms underlying rhinosinusitis  
485 with polyps and asthma, the resultant changes in cellular states and their frequencies in  
486 airway wall differ considerably between the epithelia of the upper *versus* the lower airways.  
487 In contrast, the changes in the eicosanoid pathway observed in chronic type-2 inflammation  
488 of the upper<sup>27</sup> and lower (extended data Figure 10) airways are very similar, likely reflecting  
489 a common cellular mechanism between Th2 inflammation in these two anatomical locations.

490

491 Conflicting data have been reported on dependence of IL13-induced goblet cell metaplasia  
492 on NOTCH signalling in *ex vivo* cultured PBECs<sup>25,46</sup>. Our data on freshly isolated bronchial

493 epithelial cells show that expression of NOTCH2 and Notch target genes is present in goblet  
494 cells from healthy controls only, and absent from ciliated, mucous ciliated and goblet cells  
495 in asthmatic airway wall. This indicates that mucous cell metaplasia in mild asthmatics is  
496 likely to be driven by type-2 cytokines in a NOTCH-independent fashion. One likely source  
497 of the type-2 cytokines driving this goblet cell metaplasia are the cytokine-expressing  
498 effector Th2 cells that are increased in asthmatic airway wall. To our knowledge, our study  
499 is the first to conclusively show the presence of the recently identified<sup>39,40,41</sup> pathogenic  
500 effector Th2 cells in the airway wall in asthma, as evidenced by the combined expression of  
501 *IL5*, *IL13*, *HPGDS*, *PPARG*, *IL17RB*, *IL1RL1* and *IL1RAP*. Additional cellular sources for the  
502 type-2 cytokines, including innate lymphoid cells, cannot be ruled out based on our data, as  
503 these cells were present in too low numbers to be analysed in our dataset, and will need to  
504 be purified from the biopsy cell suspensions for further characterization in future studies.  
505

506 Finally, our detailed and unbiased analyses of cell-cell communication in healthy and  
507 asthmatic airway wall reveals novel interactions of the airway wall resident cells in health  
508 and disease. Comprehensive analysis of the cell-cell interactions underpinning the changes  
509 of the airway wall cellular landscape in asthma identifies a shift away from interactions  
510 between structural cells in healthy airway wall, towards an intercellular network dominated  
511 by the interactions of Th2 cells with structural and inflammatory cells in asthmatic airway  
512 wall. The richness of growth factor signalling between epithelial cells and mesenchymal cells  
513 observed in healthy airway wall is largely lost in asthma, which seems at odds with a  
514 reactivation of the epithelial-mesenchymal trophic unit in asthma<sup>47</sup>. Instead, our data  
515 supports a shift in cellular phenotypes in airway wall due to the local production of Th2  
516 cytokines such as IL13 in chronic disease in our patient cohort with childhood-onset asthma.  
517 This global view of the airway wall cellular landscape in health and in asthma opens up new  
518 perspectives on lung biology and molecular mechanisms of asthma.  
519



520 **Acknowledgments:**

521 We thank Jana Elias (scientific illustrator) for the design of cartoons, the Sanger Single Cell  
522 Genomics Core Facility for support with the SmartSeq2 protocol, Dr. Emma Rawlins for  
523 feedback and critical reading of the manuscript, as well as all the members of the Teichmann  
524 lab for scientific input. We are grateful to the Cambridge Biorepository for Translational  
525 Medicine for the provision of tissue from deceased organ donors.

526  
527 **Authors contribution:**

528  
529 Designed the project: Teichmann, S.A, Nawijn, M.C., van den Berge, M., Affleck, K., van  
530 Oosterhout, A.J., Schiller, H.B. Wrote the paper: Vieira Braga, F.A., Nawijn, M.C.,  
531 Teichmann, S.A. Generated data: Vieira Braga, F.A., Carpaij, O.A., Brouwer, S., Hesse, L.,  
532 Jiang, J., Fasouli, E.S., Strzelecka, P., Mahbubani, K.T.A., Angelidis, I., Strunz, M. Analysed  
533 data: Vieira Braga, F.A., Kar, G., Berg, M. Simon, L., Gomes, T., Jiang, J., Efremova, M.,  
534 Palit, S., Polanski, K., Firth, H.V., Theis, F.J. Interpreted data: Vieira Braga, F.A., Kar, G.,  
535 Carpaij, O.A., Simon, L., Gomes, T., Jiang, J., Vento-Tormo, R., Affleck, K., Palit, S., Cvejic,  
536 A., Saeb-Parsy, K., Timens, W., Koppelman, G.H., van Oosterhout, A.J., Schiller, H.B., van  
537 den Berge, M., Theis, F.J., van den Berge, M., Meyer, K.B. All authors read the manuscript,  
538 offered feedback and approved it prior to submission.

539  
540 **Funding:**

541 This work was funded by Open Targets, an open innovation public-private partnership  
542 (<http://www.opentargets.org>), a GlaxoSmithKline collaborative agreement with University  
543 Medical Center Groningen, Wellcome (WT206194), EMBO and HFSP Long Term  
544 fellowships to R. Vento-Tormo, the Marie Curie ENLIGHT-TEN training network for Tomas  
545 Gomes, the Lung Foundation Netherlands (projects no 5.1.14.020 and 4.1.18.226), and  
546 Health-Holland, Top Sector Life Sciences & Health. LMS acknowledges funding from the  
547 European Union's Horizon 2020 research and innovation programme under the Marie  
548 Sklodowska-Curie grant agreement No 753039.

549  
550 **Competing interests.**

551 Affleck, K and van Oosterhout, A.J are employees of GSK.

552  
553 **Data availability:**

554 Interactive exploration tool: [www.lungcellatlas.org](http://www.lungcellatlas.org)

555  
556 **Materials & Correspondence.**

557 [m.c.nawijn@umcg.nl](mailto:m.c.nawijn@umcg.nl), [st9@sanger.ac.uk](mailto:st9@sanger.ac.uk)

558

559

## 560 References

- 561 1. Bousquet, J., Dahl, R. & Khaltaev, N. Global Alliance against Chronic Respiratory Diseases.  
562 *Eur. Respir. J.* **29**, 233–239 (2007).
- 563 2. Regev, A. *et al.* The Human Cell Atlas. *Elife* **6**, (2017).
- 564 3. Franks, T. J. *et al.* Resident cellular components of the human lung: current knowledge and  
565 goals for research on cell phenotyping and function. *Proc. Am. Thorac. Soc.* **5**, 763–766  
566 (2008).
- 567 4. Montoro, D. T. *et al.* A revised airway epithelial hierarchy includes CFTR-expressing  
568 ionocytes. *Nature* **560**, 319–324 (2018).
- 569 5. Plasschaert, L. W. *et al.* A single-cell atlas of the airway epithelium reveals the CFTR-rich  
570 pulmonary ionocyte. *Nature* **560**, 377–381 (2018).
- 571 6. Tata, P. R. & Rajagopal, J. Plasticity in the lung: making and breaking cell identity.  
572 *Development* **144**, 755–766 (2017).
- 573 7. Macosko, E. Z. *et al.* Highly Parallel Genome-wide Expression Profiling of Individual Cells  
574 Using Nanoliter Droplets. *Cell* **161**, 1202–1214 (2015).
- 575 8. Mereu, E. *et al.* matchScore: Matching Single-Cell Phenotypes Across Tools and  
576 Experiments. *bioRxiv* 314831 (2018). doi:10.1101/314831
- 577 9. Bisset, L. R. & Schmid-Grendelmeier, P. Chemokines and their receptors in the pathogenesis  
578 of allergic asthma: progress and perspective. *Curr. Opin. Pulm. Med.* **11**, 35–42 (2005).
- 579 10. Colvin, R. A. *et al.* Synaptotagmin-mediated vesicle fusion regulates cell migration. *Nat.*  
580 *Immunol.* **11**, 495–502 (2010).
- 581 11. Urawa, M. *et al.* Protein S is protective in pulmonary fibrosis. *J. Thromb. Haemost.* **14**, 1588–  
582 1599 (2016).
- 583 12. Wujak, Ł. A. *et al.* FXYP1 negatively regulates Na(+)/K(+)-ATPase activity in lung alveolar  
584 epithelial cells. *Respir. Physiol. Neurobiol.* **220**, 54–61 (2016).
- 585 13. Krotova, K. *et al.* Alpha-1 Antitrypsin-Deficient Macrophages Have Increased Matriptase-  
586 Mediated Proteolytic Activity. *Am. J. Respir. Cell Mol. Biol.* **57**, 238–247 (2017).
- 587 14. Vogl, T. *et al.* S100A12 is expressed exclusively by granulocytes and acts independently from  
588 MRP8 and MRP14. *J. Biol. Chem.* **274**, 25291–25296 (1999).
- 589 15. Mitchell, A. *et al.* LILRA5 is expressed by synovial tissue macrophages in rheumatoid arthritis,  
590 selectively induces pro-inflammatory cytokines and IL-10 and is regulated by TNF-alpha, IL-10  
591 and IFN-gamma. *Eur. J. Immunol.* **38**, 3459–3473 (2008).
- 592 16. Condon, T. V., Sawyer, R. T., Fenton, M. J. & Riches, D. W. H. Lung dendritic cells at the  
593 innate-adaptive immune interface. *J. Leukoc. Biol.* **90**, 883–895 (2011).
- 594 17. Holgate, S. T. *et al.* Asthma. *Nat Rev Dis Primers* **1**, 15025 (2015).
- 595 18. Lopez-Guisa, J. M. *et al.* Airway epithelial cells from asthmatic children differentially express  
596 proremodeling factors. *J. Allergy Clin. Immunol.* **129**, 990–7.e6 (2012).
- 597 19. Alcalá, S. E. *et al.* Mitotic asynchrony induces transforming growth factor-β1 secretion from  
598 airway epithelium. *Am. J. Respir. Cell Mol. Biol.* **51**, 363–369 (2014).
- 599 20. Harkness, L. M., Ashton, A. W. & Burgess, J. K. Asthma is not only an airway disease, but  
600 also a vascular disease. *Pharmacol. Ther.* **148**, 17–33 (2015).
- 601 21. Balzar, S. *et al.* Mast cell phenotype, location, and activation in severe asthma. Data from the  
602 Severe Asthma Research Program. *Am. J. Respir. Crit. Care Med.* **183**, 299–309 (2011).
- 603 22. Truyen, E. *et al.* Evaluation of airway inflammation by quantitative Th1/Th2 cytokine mRNA  
604 measurement in sputum of asthma patients. *Thorax* **61**, 202–208 (2006).
- 605 23. Trapnell, C. *et al.* The dynamics and regulators of cell fate decisions are revealed by  
606 pseudotemporal ordering of single cells. *Nat. Biotechnol.* **32**, 381–386 (2014).
- 607 24. Erle, D. J. & Sheppard, D. The cell biology of asthma. *J. Cell Biol.* **205**, 621–631 (2014).
- 608 25. Danahay, H. *et al.* Notch2 is required for inflammatory cytokine-driven goblet cell metaplasia in  
609 the lung. *Cell Rep.* **10**, 239–252 (2015).
- 610 26. Gomi, K., Arbelaez, V., Crystal, R. G. & Walters, M. S. Activation of NOTCH1 or NOTCH3  
611 signalling skews human airway basal cell differentiation toward a secretory pathway. *PLoS*  
612 *One* **10**, e0116507 (2015).
- 613 27. Ordovas-Montanes, J. *et al.* Allergic inflammatory memory in human respiratory epithelial  
614 progenitor cells. *Nature* **560**, 649–654 (2018).
- 615 28. Luo, W. *et al.* Airway Epithelial Expression Quantitative Trait Loci Reveal Genes Underlying

- 616 Asthma and Other Airway Diseases. *Am. J. Respir. Cell Mol. Biol.* **54**, 177–187 (2016).
- 617 29. Wu, C. A. *et al.* Bronchial epithelial cells produce IL-5: implications for local immune  
618 responses in the airways. *Cell. Immunol.* **264**, 32–41 (2010).
- 619 30. Laitinen, L. A., Laitinen, A. & Haahtela, T. Airway mucosal inflammation even in patients with  
620 newly diagnosed asthma. *Am. Rev. Respir. Dis.* **147**, 697–704 (1993).
- 621 31. Arima, M. & Fukuda, T. Prostaglandin D2 and TH2 Inflammation in the Pathogenesis of  
622 Bronchial Asthma. *Korean J. Intern. Med.* **26**, 8 (2011).
- 623 32. Xue, L. *et al.* Prostaglandin D2 activates group 2 innate lymphoid cells through  
624 chemoattractant receptor-homologous molecule expressed on TH2 cells. *J. Allergy Clin.*  
625 *Immunol.* **133**, 1184–1194 (2014).
- 626 33. Dougherty, R. H. *et al.* Accumulation of intraepithelial mast cells with a unique protease  
627 phenotype in T(H)2-high asthma. *J. Allergy Clin. Immunol.* **125**, 1046–1053.e8 (2010).
- 628 34. Hol, B. E., van de Graaf, E. A., Out, T. A., Hische, E. A. & Jansen, H. M. IgM in the airways of  
629 asthma patients. *Int. Arch. Allergy Appl. Immunol.* **96**, 12–18 (1991).
- 630 35. Peebles, R. S., Jr, Liu, M. C., Lichtenstein, L. M. & Hamilton, R. G. IgA, IgG and IgM  
631 quantification in bronchoalveolar lavage fluids from allergic rhinitics, allergic asthmatics, and  
632 normal subjects by monoclonal antibody-based immunoenzymetric assays. *J. Immunol.*  
633 *Methods* **179**, 77–86 (1995).
- 634 36. Muehling, L. M., Lawrence, M. G. & Woodfolk, J. A. Pathogenic CD4+ T cells in patients with  
635 asthma. *J. Allergy Clin. Immunol.* **140**, 1523–1540 (2017).
- 636 37. Oja, A. E. *et al.* Trigger-happy resident memory CD4+ T cells inhabit the human lungs.  
637 *Mucosal Immunol.* **11**, 654–667 (2018).
- 638 38. Kumar, B. V. *et al.* Human Tissue-Resident Memory T Cells Are Defined by Core  
639 Transcriptional and Functional Signatures in Lymphoid and Mucosal Sites. *Cell Rep.* **20**,  
640 2921–2934 (2017).
- 641 39. Mitson-Salazar, A. *et al.* Hematopoietic prostaglandin D synthase defines a proeosinophilic  
642 pathogenic effector human T(H)2 cell subpopulation with enhanced function. *J. Allergy Clin.*  
643 *Immunol.* **137**, 907–18.e9 (2016).
- 644 40. Wambre, E. *et al.* A phenotypically and functionally distinct human TH2 cell subpopulation is  
645 associated with allergic disorders. *Sci. Transl. Med.* **9**, (2017).
- 646 41. Lam, E. P. S. *et al.* IL-25/IL-33-responsive TH2 cells characterize nasal polyps with a default  
647 TH17 signature in nasal mucosa. *J. Allergy Clin. Immunol.* **137**, 1514–1524 (2016).
- 648 42. Vento-Tormo, R. *et al.* Single-cell reconstruction of the early maternal–fetal interface in  
649 humans. *Nature* **563**, 347–353 (2018).
- 650 43. Weckmann, M., Kopp, M. V., Heinzmann, A. & Mattes, J. Haplotypes covering the TNFSF10  
651 gene are associated with bronchial asthma. *Pediatr. Allergy Immunol.* **22**, 25–30 (2011).
- 652 44. Harada, M. *et al.* Thymic stromal lymphopoietin gene promoter polymorphisms are associated  
653 with susceptibility to bronchial asthma. *Am. J. Respir. Cell Mol. Biol.* **44**, 787–793 (2011).
- 654 45. Grotenboer, N. S., Ketelaar, M. E., Koppelman, G. H. & Nawijn, M. C. Decoding asthma:  
655 translating genetic variation in IL33 and IL1RL1 into disease pathophysiology. *J. Allergy Clin.*  
656 *Immunol.* **131**, 856–865 (2013).
- 657 46. Gerovac, B. J. & Fregien, N. L. IL-13 Inhibits Multicilin Expression and Ciliogenesis via Janus  
658 Kinase/Signal Transducer and Activator of Transcription Independently of Notch Cleavage.  
659 *Am. J. Respir. Cell Mol. Biol.* **54**, 554–561 (2016).
- 660 47. Holgate, S. T. *et al.* Epithelial-mesenchymal communication in the pathogenesis of chronic  
661 asthma. *Proc. Am. Thorac. Soc.* **1**, 93–98 (2004).
- 662 48. Butler, A., Hoffman, P., Smibert, P., Papalexi, E. & Satija, R. Integrating single-cell  
663 transcriptomic data across different conditions, technologies, and species. *Nat. Biotechnol.* **36**,  
664 411–420 (2018).
- 665 49. Song, J. *et al.* Aberrant DNA methylation and expression of SPDEF and FOXA2 in airway  
666 epithelium of patients with COPD. *Clin. Epigenetics* **9**, 42 (2017).
- 667 50. Heijink, I. H. *et al.* Down-regulation of E-cadherin in human bronchial epithelial cells leads to  
668 epidermal growth factor receptor-dependent Th2 cell-promoting activity. *J. Immunol.* **178**,  
669 7678–7685 (2007).
- 670 51. Picelli, S. *et al.* Full-length RNA-seq from single cells using Smart-seq2. *Nat. Protoc.* **9**, 171–  
671 181 (2014).
- 672 52. Wu, T. D. & Nacu, S. Fast and SNP-tolerant detection of complex variants and splicing in short

- 673 reads. *Bioinformatics* **26**, 873–881 (2010).  
674 53. Dobin, A. *et al.* STAR: ultrafast universal RNA-seq aligner. *Bioinformatics* **29**, 15–21 (2013).  
675 54. van den Brink, S. C. *et al.* Single-cell sequencing reveals dissociation-induced gene  
676 expression in tissue subpopulations. *Nat. Methods* **14**, 935–936 (2017).  
677 55. Young, M. D. & Behjati, S. SoupX removes ambient RNA contamination from droplet based  
678 single cell RNA sequencing data. *bioRxiv* (2018).

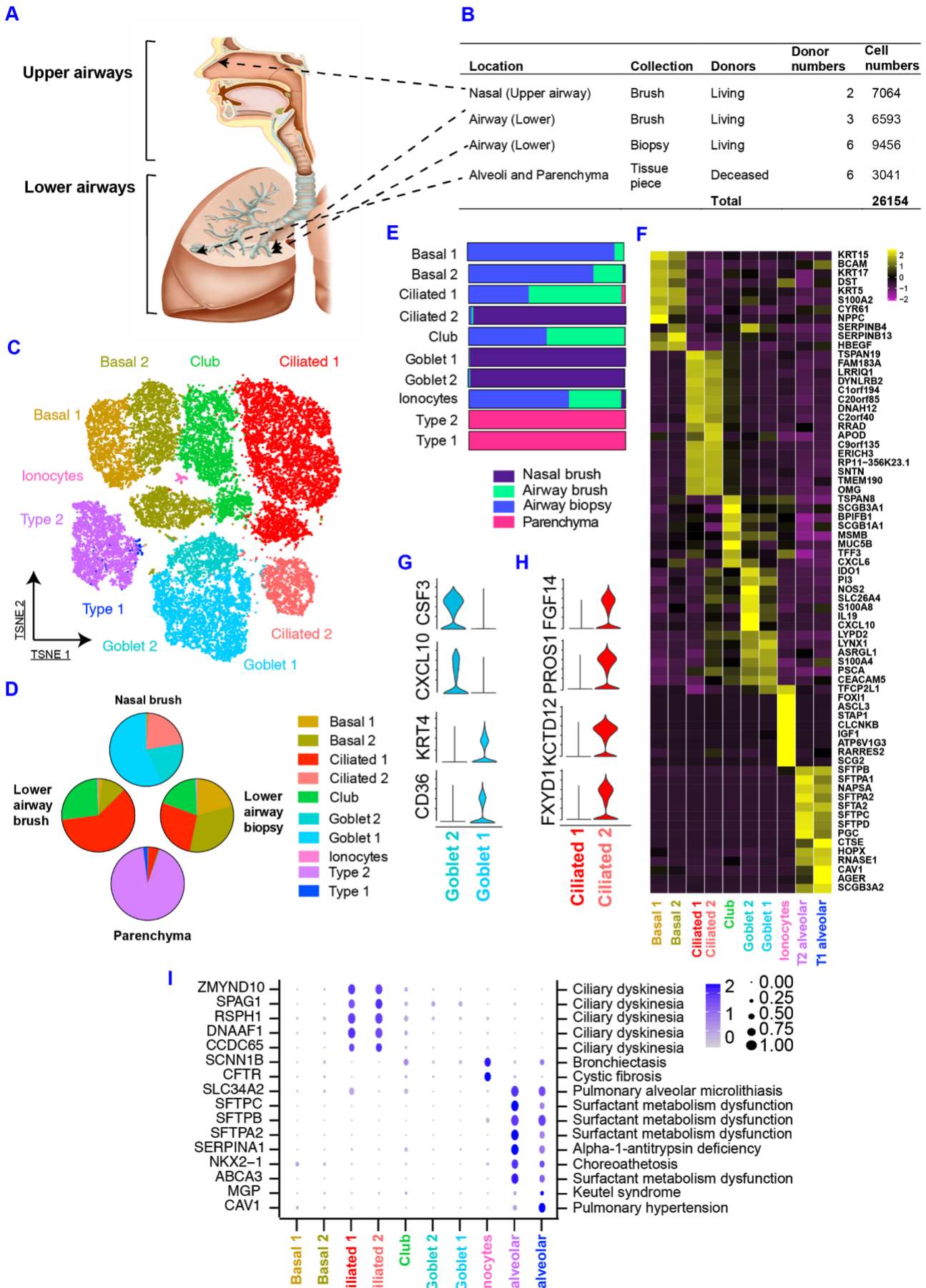
679

680

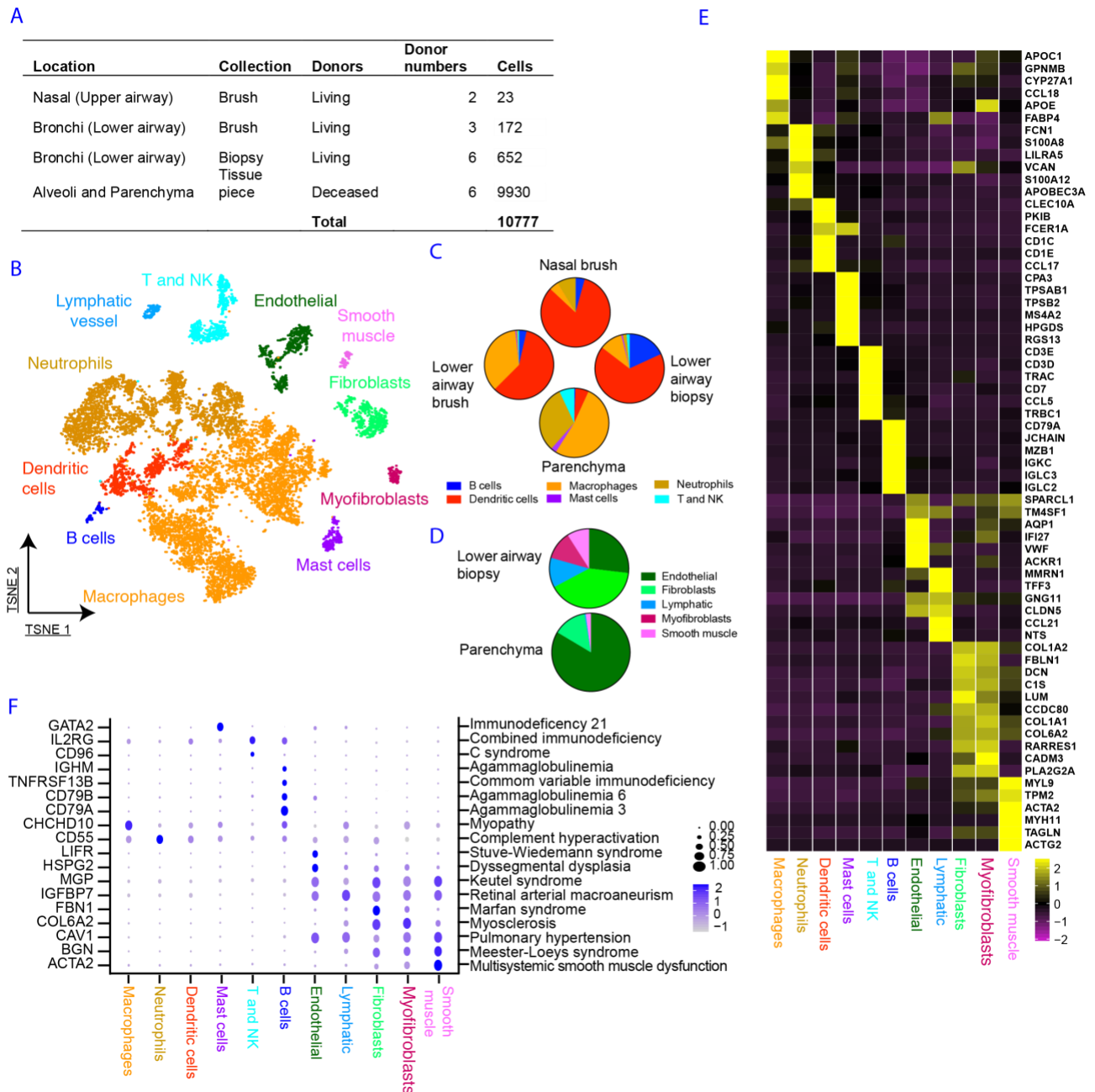
681

682

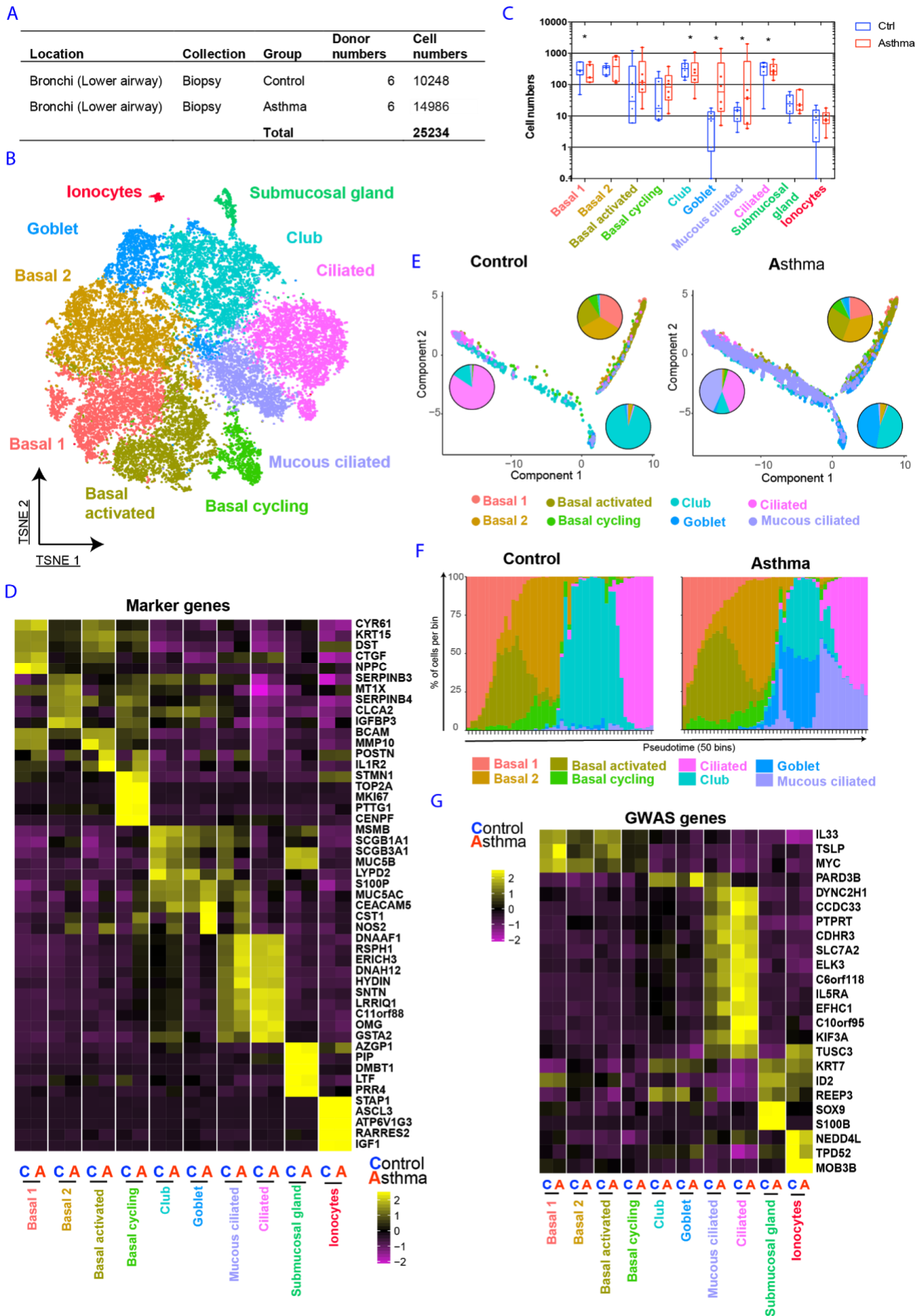




684 **Figure 1. A human lung cell census identifies zonation of novel epithelial cell states**  
685 **across macro-anatomical location. (A)** Schematic illustration depicting anatomical  
686 regions analysed in this manuscript. **(B)** Table with the details of anatomical region, tissue  
687 source, donors and cell numbers present in this figure. **(C)** tSNE displaying the major  
688 epithelial clusters present in the full extent of the human respiratory tree. **(D)** Pie charts  
689 depicting the cellular composition by anatomical region. **(E)** Horizontal slice bar depicting  
690 the anatomical distribution of each cell type identified **(F)** Heatmap depicting the average  
691 expression levels per cluster of the top differentially expressed markers in each cluster. **(G)**  
692 Violin plots of selected markers identified by differential expression analysis comparing the  
693 two goblet subsets to each other. **(H)** Violin plots of selected markers identified by differential  
694 expression analysis of ciliated 1 versus ciliated 2 clusters. **(I)** Dot plot depicting gene  
695 expression levels and percentage of cells expressing genes associated with specific lung  
696 phenotypes according to the Online Mendelian Inheritance in Man (OMIM) database. Only  
697 genes present in the top 50 (per cluster) of our list of differentially expressed genes are  
698 depicted in (I). All the differential expression analysis were performed using Wilcoxon rank  
699 sum test in Seurat<sup>48</sup>.  
700



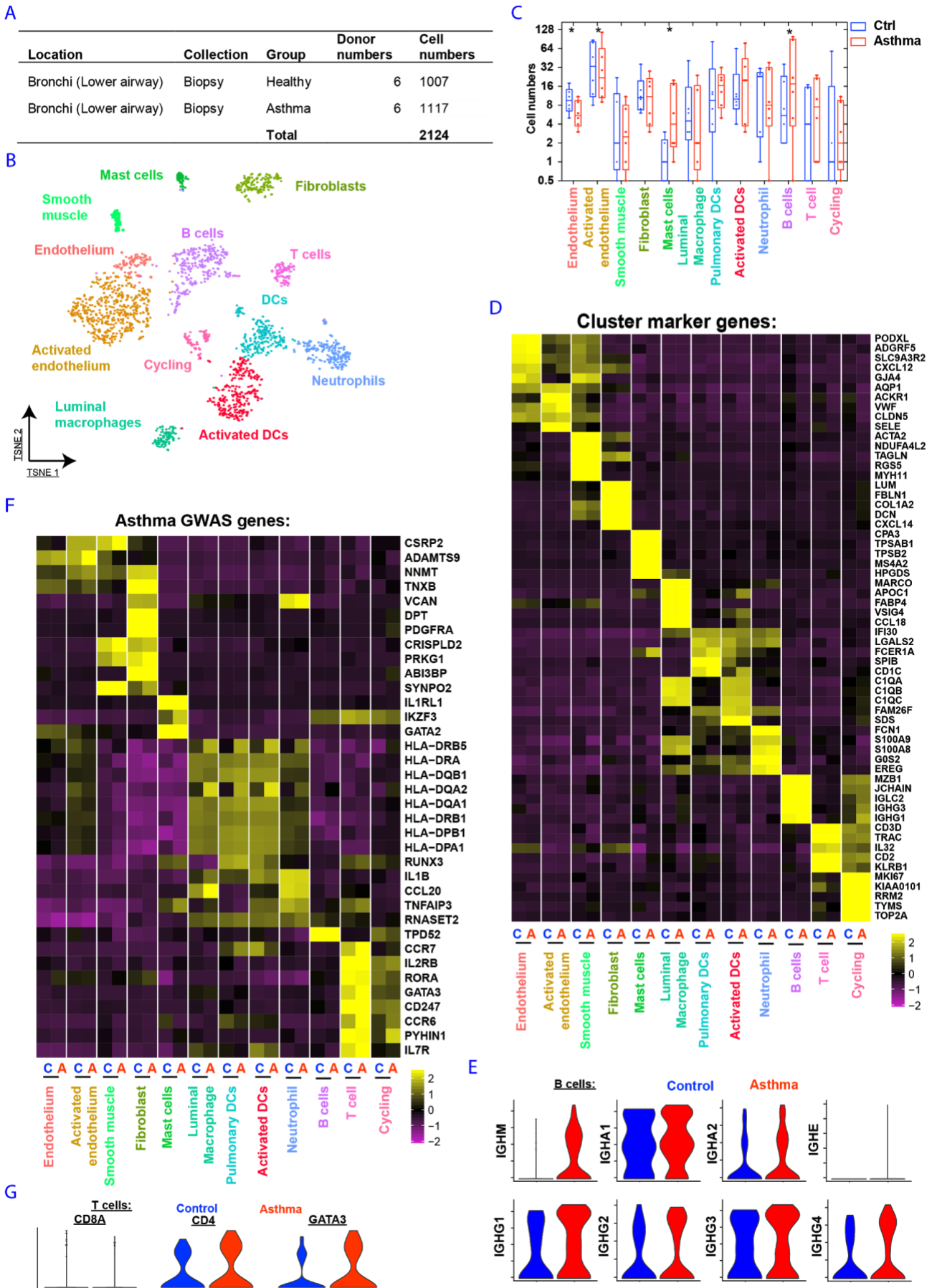
701  
 702 **Figure 2. A cellular and molecular map of the stromal and immune components of**  
 703 **across the upper and lower human respiratory airways. (A)** Table with details of  
 704 anatomical region, tissue source, donors and cell numbers present in this figure. **(B)**  
 705 tSNE displaying the major immune and mesenchymal clusters present in the full extent of the  
 706 human respiratory tree. **(C)** Pie charts depicting the cellular composition of immune cells by  
 707 anatomical region. **(D)** Pie charts depicting the cellular composition of stromal cells in lower  
 708 airway biopsies and parenchyma tissue. **(E)** Heatmap depicting the average expression  
 709 levels per cluster of the top differentially expressed markers in each cluster. **(F)** Dot plot  
 710 depicting gene expression levels and percentage of cells expressing genes associated with  
 711 lung phenotypes according to the Online Mendelian Inheritance in Man (OMIM) database.  
 712 Only genes present in the top 50 (per cluster) of our list of differentially expressed genes are  
 713 depicted in (F). All the differential expression analysis was performed using Wilcoxon rank  
 714 sum test in Seurat.





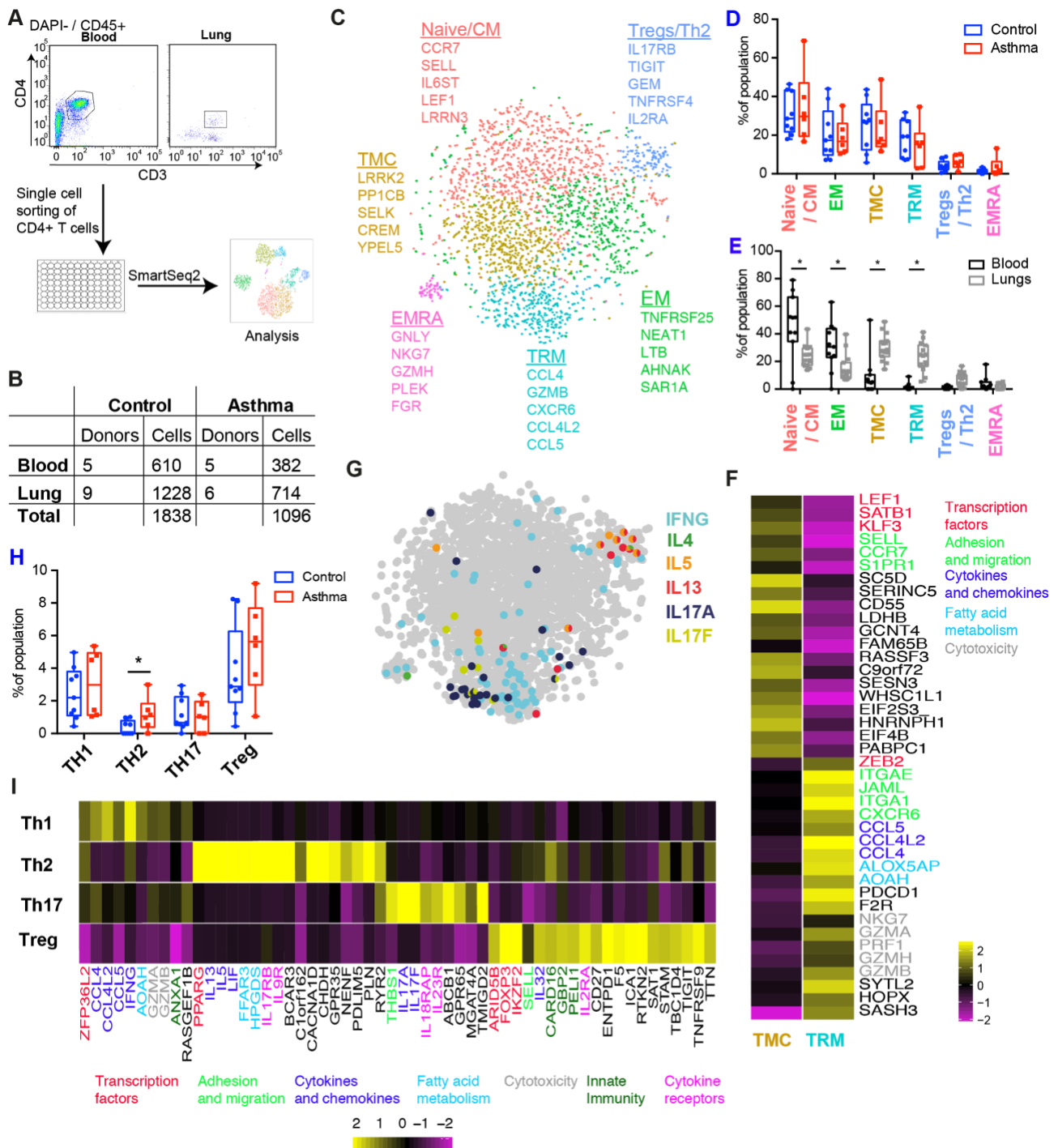
716 **Figure 3. Distinct programs of epithelial cell differentiation in asthmatic versus**  
717 **healthy airways. (A)** Table with overview and cell numbers for control and asthma  
718 volunteers analysed in this figure. **(B)** tSNE displaying all epithelial cells analysed coloured  
719 by their specific cluster assignment. **(C)** Box and whisker plots depicting cell numbers of  
720 control and asthma patients in each cluster. **(D)** Heatmap displaying the top five differentially  
721 expressed genes per cluster. **(E)** Pseudotime developmental trajectory analysis from  
722 Monocle2 depicting how each of the basal, secretory and ciliated subsets relate to each  
723 other. **(F)** Binned pseudotime analysis displaying how each subset is ordered in a one-  
724 dimensional continuous space. **(G)** Heatmap displaying the expression of asthma genes  
725 from GWAS. Only genes present in our list of differentially expressed genes are depicted  
726 for each cell cluster. Significance analysed using Fisher's exact test corrected for multiple  
727 comparison using the Bonferroni method. Significance calculated using all the clusters  
728 present in figures 3 and 4, which were derived from the same set of samples. \*represents  
729 p-value<0.001. n=6 controls and n=6 asthma. The differential expression analysis used for  
730 input in D and E was performed using Wilcoxon rank sum test in Seurat.  
731

732



733

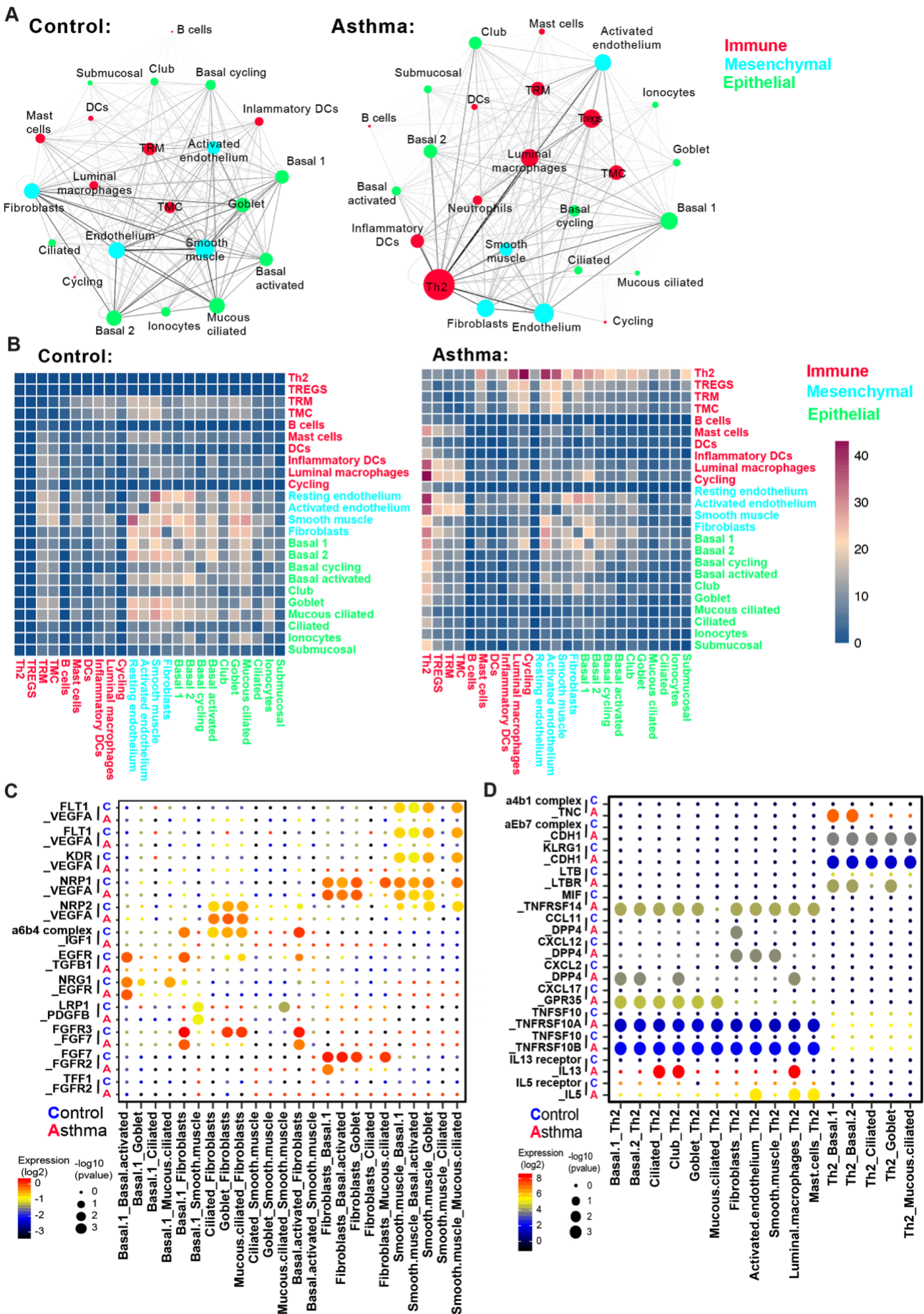
734 **Figure 4. Remodelling of the stromal and Immune compartments in asthmatic**  
735 **airways. (A)** Table with the number of donors and cells per volunteer group included in this  
736 figure. **(B)** tSNE depicting the immune and stromal cell types identified in the human airway  
737 combined dataset of healthy and asthmatic patients. **(C)** Box and whisker plots depicting the  
738 cell numbers of healthy and asthmatic cells in each cluster. **(D)** Heatmap displaying gene  
739 expression levels of the top 5 differentially expressed genes per cluster. **(E)** Violin plots  
740 depicting expression of immunoglobulin genes in B cells. **(F)** Heatmap displaying asthma  
741 GWAS gene expression per cluster. Only genes present in the top 50 (per cluster) of our list  
742 of differentially expressed genes are shown. **(G)** Violin plots of selected T cell markers in  
743 asthma patients. Significance calculated using all the clusters present in figures 3 and 4,  
744 which were derived from the same set of samples. \*represents p-value<0.001. n=6 controls  
745 and n=6 asthma.  
746  
747  
748



749  
 750 **Figure 5. Pathogenic effector Th2 cells are enriched in asthmatic airways.** (A)  
 751 Schematic depicting experimental layout of single cell sorting of CD4 T cells from blood and  
 752 lung airway biopsies. (B) Table with the number of donors by anatomical location for control  
 753 and asthma groups. (C) tSNE displaying clusters of T cells identified by analysing the  
 754 combined cells from blood and lung from control and asthma groups. (D) Box and whisker  
 755 plots showing the cluster cell distributions from control and asthma patients. (E) Box and  
 756 whisker plots depicting the cluster composition per donor according to the tissue source from  
 757 which the cells were isolated. (F) Heatmap showing the average expression per cluster of  
 758 genes differentially expressed between the two lung specific CD4 T cell populations. Gene  
 759 names coloured according to functional categories. (G) tSNE depicting canonical cytokines  
 760 from Th1, Th2 and Th17 cells. (H) Box and whisker plots showing the number of Th1, Th2  
 761 and Th17 cells defined by canonical cytokines expression and Tregs identified by unbiased  
 762 clustering. (I) Heatmap of average cluster gene expression of markers differentially

763 expressed between Th1, Th2, Th17 and Treg cells. Gene names coloured according to  
764 functional categories. Error bars in **(D)**, **(E)** and **(H)** represent standard deviation.  
765 Significance analysed using Multiple t-tests corrected for multiple comparison using the  
766 Holm-Sidak method. \* represents p-value<0.05. Patient numbers per tissue depicted in (B).  
767  
768  
769





770  
771  
772

**Figure 6. Asthma is characterized by unique cell-to-cell signalling networks.** We quantified the predicted cell interactions in healthy and asthmatic airways between all the

773 epithelial and non-epithelial cell clusters identified in figures 3 and 4, plus the lung airway  
774 enriched populations of CD4 T cells (Th2, Treg, TMC and TRM) **(A)** Networks depicting cell  
775 types as nodes and interactions as edges. Size of cell type proportional to the total number  
776 of interactions of each cell type and edge thickness proportional to the number of interactions  
777 between the connecting types. **(B)** Heatmap depicting the number of all possible interactions  
778 between the clusters analysed. Cell types grouped by broad lineage (epithelia,  
779 mesenchymal or immune). **(C)** Dot plot depicting selected epithelial-epithelial and epithelial-  
780 mesenchymal interactions enriched in healthy airways but absent in asthma. **(D)** Dot plot  
781 depicting selected epithelial-immune and mesenchymal-immune interactions highly  
782 enriched in asthma but absent in healthy airways.

783 **Methods**

784

785 **Patient recruitment and ethical approval**

786 Bronchoscopy biopsy (10x and smartseq2 analysis): cohort inclusion criteria for all subjects  
 787 were: age between 40 – 65 years and history of smoking <10 pack years. For the asthmatics,  
 788 inclusion criteria were: age of onset of asthmatic symptoms ≤12 years, documented history  
 789 of asthma, use of inhaled corticosteroids with(out) β2-agonists due to respiratory symptoms  
 790 and a positive provocation test (i.e. PC<sub>20</sub> methacholine ≤8mg/ml with 2-minute protocol). For  
 791 the non-asthmatic controls, the following criteria were essential for inclusion: absent history  
 792 of asthma, no use of asthma-related medication, a negative provocation test (i.e. PC<sub>20</sub>  
 793 methacholine >8 mg/ml and adenosine 5'-monophosphate >320 mg/ml with 2-minute  
 794 protocol), no pulmonary obstruction (i.e. FEV<sub>1</sub>/FVC ≥70%) and absence of lung function  
 795 impairment (i.e. FEV<sub>1</sub> ≥80% predicted).

796 Asthmatics stopped inhaled corticosteroid use 6 weeks prior to all tests. All subjects were  
 797 clinically characterised with pulmonary function and provocation tests, blood samples were  
 798 drawn, and finally subjects underwent a bronchoscopy under sedation. If a subject  
 799 developed upper respiratory symptoms, bronchoscopy was postponed for ≥6 weeks.

800 Fibreoptic bronchoscopy was performed using a standardised protocol during conscious  
 801 sedation [1]. Six macroscopically adequate endobronchial biopsies were collected for this  
 802 study, located between the 3<sup>rd</sup> and 6<sup>th</sup> generation of the right lower and middle lobe.  
 803 Extracted biopsies were processed directly thereafter, with a maximum of one hour delay.  
 804 The medical ethics committee of the Groningen University Medical Center Groningen  
 805 approved the study, and all subjects gave their written informed consent. Detailed patient  
 806 information below:  
 807

Donor	Gender	Age	Classification	Packyears	BMI	FEV1% pred	FEV1/FVC ratio	PC20 methacholine threshold (mg/ml)	10x	Smartseq2
ARMS004	F	57	Ctrl	0	21	99	82	Not reached	no	yes
ARMS005	F	44	Ctrl	4	24	111	82	Not reached	no	yes
ARMS009	M	49	Asthma	0	22	87	69	0.211	no	yes
ARMS014	F	65	Ctrl	0	18	109	78	Not reached	no	yes
ARMS015	M	49	Asthma	0	24	105	67	1.155	no	yes
ARMS018	M	54	Ctrl	3	25	107	80	Not reached	no	yes
ARMS019	F	56	Asthma	0	45	44	55	FEV1 too low	no	yes
ARMS022	M	48	Ctrl	1	30	131	84	Not reached	no	yes
ARMS024	F	51	Asthma	0	33	96	74	0.88	yes	yes
ARMS026	M	64	Ctrl	5	32	103	81	Not reached	yes	yes
ARMS032	M	56	Ctrl	0	22	120	75	Not reached	yes	yes
ARMS033	M	51	Asthma	0	23	98	69	2.63	yes	yes
ARMS035	M	61	Asthma	0	20	89	59	6.71	yes	yes
ARMS038	M	59	Ctrl	0	23	148	74	Not reached	yes	yes
ARMS040	M	51	Ctrl	0	23	119	73	Not reached	yes	yes
ARMS043	F	50	Ctrl	1	23	110	71	Not reached	yes	no
ARMS048	M	53	PersA	0	29	77	54	0.205	yes	no
ARMS050	M	64	PersA	0	21	85	66	0.692	yes	no
ARMS051	M	64	PersA	0	25	59	54	0.631	yes	no
ARMS054	M	60	Ctrl	0	29	116	81	Not reached	yes	no

808

809

810

811 Lung resection (Dropseq analysis): Fresh resected human lung tissue (parenchymal lung  
 812 and distal airway specimens) was obtained via the CPC BioArchive at the Comprehensive  
 813 Pneumology Center Munich (CPC-M, Munich, Germany). In total, we analysed parenchymal  
 814 tissue of uninvolved areas of tumour resection material from four patients. All participants  
 815 gave written informed consent and the study was approved by the local ethics committee of  
 816 the Ludwig-Maximilians University of Munich, Germany.

817 For transport from the surgeon to the laboratory, lung tissue samples were stored in ice-cold  
 818 DMEM-F12 media and packed in thermo stable boxes. Tissue was processed with a  
 819 maximum delay of 2 hours after surgery. Upon delivery to the lab, tissue samples were  
 820 assessed visually for qualification for the study.

821 Donor information:

822

ID	Sample	Gender	Age	Smoker	Segment	COPD
muc3843	ASK428	m	62	yes, >100py	lower lobe, left	COPD Gold II
muc4658	ASK440	m	58	yes, 45py	upper lobe, left	no
muc5103	ASK452	m	58	no	main bronchus	no
muc5104	ASK454	m	69	yes, >60py	upper lobe, left	no

823 Lung transplant tissue (10x analysis): Human lung tissue was obtained from deceased organ  
824 donors from whom organs were being retrieved for transplantation. Informed consent for the  
825 use of tissue was obtained from the donors' families (REC reference: 15/EE/0152 NRES  
826 Committee East of England - Cambridge South).

827 Fresh tissue from the peripheral parenchyma of the left lower lobe or lower right lobe of the  
828 lung was excised within 60 minutes of circulatory arrest and preserved in University of  
829 Wisconsin (UW) organ preservation solution (Belzer UW® Cold Storage Solution, Bridge to  
830 Life, USA) until processing.

831

832 Donor information:

833

834 *Donor 284C*

835 Gender: Male

836 Age band: 55-60

837 BMI: 25.83

838 Cause of Death: hypoxic brain damage

839 Smoking history: smoked 20/day for 25 years

840 Stopped: 08/2000

841 Respiratory related information: Chest X-ray normal on admission. No pleural effusion or  
842 pneumothorax. Not diagnosed with asthma, but inhalers for possible seasonal wheeze.  
843 Family report only using inhaler approximately 5 times a year. No recent peak flow on record  
844 last one in 2008 when it was 460, predicted is 611.

845 Time from death to cell lysis: 12h

846

847 *Donor 290B*

848 Gender: Female

849 Age band: 60-65

850 BMI: 27.77

851 Cause of Death: hypoxic brain damage

852 Smoking history: smoked 15/day for 7 years

853 Stopped: no details

854 Respiratory related information: Respiratory tests all normal on admission; maintaining own  
855 airway. GP notes report Acute bronchitis in 1994.

856 Time from death to cell lysis: 2h 27min

857

858 *Donor: 292B*

859 Gender: Male

860 Age band: 55-60

861 BMI: 27.44

862 Cause of Death: Intracranial haemorrhage

863 Smoking history: smoked 20/day for 46 years  
864 Stopped: no details  
865 Respiratory related information: Chest X-ray normal on admission, lungs appear clear.  
866 Bronchoscopy results show global inflamed mucosa. No other history of respiratory issues.  
867 Time from death to cell lysis: 18h 50min

868  
869 *Donor: 296C*  
870 Gender: Female  
871 Age band: 30-35  
872 BMI: 20.9  
873 Cause of Death: Intracranial haemorrhage  
874 Smoking history: smoked 20/day for 19 years  
875 Stopped: no details  
876 Respiratory related information: Chest X-ray shows collapsed left lobe on admission due to  
877 consolidation. Right lobe looks normal. No history or record of respiratory issues.  
878 Time from death to cell lysis: 15h 30min

879  
880 *Donor: 298C*  
881 Gender: Male  
882 Age band: 50-55  
883 BMI: 24  
884 Cause of Death: Intracranial haemorrhage  
885 Smoking history: not available  
886 Stopped: no details  
887 Respiratory related information: no details  
888 Time from death to cell lysis: 15h 30min

889  
890 *Donor: 302C*  
891 Gender: Male  
892 Age band: 40-45  
893 BMI: 34.33  
894 Cause of Death: Known or suspected suicide  
895 Smoking history: smoked 20/day for 25 years  
896 Stopped: no details  
897 Respiratory related information: Chest X-ray shows reduced volume in right lung due to  
898 collapsed right lower lobe on admission. No history or record of respiratory issues.  
899 Time from death to cell lysis: 13h 30min

900  
901 Archived formalin-fixed paraffin-embedded (FFPE) lung blocks: Left-over frozen peripheral  
902 lung tissues from 6 current smokers and 4 non-smokers who underwent lung resection  
903 surgery. These subjects did not have a history of lung disease, apart from lung cancer for  
904 which the patients underwent surgery. Lung tissue samples were taken as distant from the  
905 tumor as possible. Thus, any possible effect of the tumor on the lung tissue was minimized.  
906 All samples were obtained according to national and local ethical guidelines and the  
907 research code of the University Medical Center Groningen.

908

<b>Bio sample code</b>	<b>Age</b>	<b>Gender</b>	<b>Smoking status</b>	<b>Diagnosis</b>
GRNG-LNG_MRK085	45	female	current smoker	LCC
GRNG-LNG_MRK125	54	female	current smoker	AC



GRNG-LNG_MRK177	52	female	current smoker	AC
GRNG-LNG_MRK188	70	male	current smoker	SCC
GRNG-LNG_MRK218	61	male	current smoker	Metastasis
GRNG-LNG_MRK245	65	female	current smoker	LCC
GRNG-LNG_0758	81	female	non-smoker	AC
GRNG-LNG_0764	49	male	non-smoker	carcinoid
GRNG-LNG_0802	50	male	non-smoker	metastasis
GRNG-LNG_0830	45	male	non-smoker	IMT

LCC = large cell carcinoma, AC = adenocarcinoma, SCC = squamous cell carcinoma and IMT = inflammatory myofibroblast tumor

909

910

### Blood processing

911

912

913

914

915

916

917

### Lung tissue processing

918

919

920

921

922

923

924

925

926

927

928

929

930

931

932

933

934

935

936

937

938

939

940

941

942

943

944

*Bronchoscopy biopsy:* A single cell solution was obtained by chopping the biopsies finely using a single edge razor blade. The chopped tissue was then put in a mixture of 1mg/ml collagenase D and 0.1mg/ml DNase I (Roche) in HBSS (Lonza). This was then placed at 37°C for 1hr with gentle agitation. The single cell suspension was forced through a 70µm nylon cell strainer (Falcon). The suspension was centrifuged at 550g, 4°C for 5 min and washed once with a PBS containing 1% BSA (Sigma Aldrich). The single cell suspensions used for 10X Genomics scRNAseq analysis were cleared of red blood cells by using a Red blood cell lysis buffer (eBioscience) followed by staining for cell surface markers.

*Lung tissue resection:* For each sample, 1-1.5 g of tissue was homogenized by mincing with scissors into smaller pieces (~0.5 mm<sup>2</sup>/piece). Prior to tissue digestion, lung homogenates were cleared from excessive blood by addition of 35 ml of ice-cold PBS, followed by gentle shaking and tissue collection using a 40µm strainer. The bloody filtrate was discarded. The tissue was transferred into 8 ml of enzyme mix consisting of dispase (50 caseinolytic U/ml), collagenase (2 mg/ml), elastase (1 mg/ml), and DNase (30 µg/ml) for mild enzymatic digestion for 1 hour at 37°C while shaking. Enzyme activity was inhibited by adding 5 ml of PBS supplemented with 10% FCS. Dissociated cells in suspension were passed through a 70µm strainer and centrifuged at 300g for 5 minutes at 4°C. The cell pellet was resuspended in 3 ml of red blood cell lysis buffer and incubated at room temperature for 2 minutes to lyse remaining red blood cells. After incubation, 10 ml of PBS supplemented with 10% FCS was added to the suspension and the mix was centrifuged at 300g for 5 minutes at 4°C. The cells were taken up in 1 ml of PBS supplemented with 10% FCS, counted using a Neubauer chamber and critically assessed for single cell separation. Dead cells were counted to calculate the overall cell viability, which needed to be above 85% to continue with Drop-Seq. 250,000 cells were aliquoted in 2.5 ml of PBS supplemented with 0.04% of bovine serum albumin and loaded for Drop-Seq at a final concentration of 100 cells/µl.

945 *Rejected lung transplant:* for each sample, 1-2g of tissue was divided in 5 smaller pieces  
946 then transferred to 5ml eppendorfs containing 1.5ml 0.5mg/ml collagenase D and 0.1mg/ml  
947 DNase I (Sigma) in RPMI. Samples were then finely minced using scissors. Minced tissue  
948 was then transferred to a petry dish and extra digestion medium added to completely cover  
949 the tissue. Samples were incubated 30min at 37°C. Cells were then passed up and down  
950 through a 16-gauge needle 10 times. Samples were incubated for an additional 15min at  
951 37°C. Cells were filtered a 70um filter, then spun down for 6min 1400RPM. 1 ml of red blood  
952 cell lysis (eBioscience) was added to the pellet during 5min. Cells were resuspended in  
953 RPMI + 10%FCS and counted. Dead cells were removed using the Dead Cell Removal Kit  
954 (Miltenyi Biotec). In brief, cells were incubated with anti-Annexin V beads for 15min. The cell  
955 suspension was then passed through a magnetic column and dead Annexin V+ cells  
956 remained in the column, while live cells were collected. Viability was then estimated *via*  
957 trypan blue. More than 99% of cells were viable.

958

### 959 **Flow cytometry**

960 Blood leukocytes were stained with CD4 APC-Cy7, CD3 PerCP Cy5.5 and CD8 APC  
961 (eBioscience) for 30min at 4°C and washed twice with PBS containing 1% BSA. Propidium  
962 iodide (PI) was added 5min before sorting.

963 Airway wall biopsy single cell suspensions were stained for 30min at 4°C with CD3 PerCP  
964 Cy5.5, CD45 BB515, CD4 APC Cy7 (BD) and CD8 PE and washed twice with PBS  
965 containing 1% BSA. Propidium iodide (IQ products) was added 5min before sorting.

966

### 967 **Cell Sorting**

968 Lymphocytes were selected in the FCS/SSC plot. These were then selected on single, live  
969 cells for blood or single, live, CD45+ for lung. The sorted cells were positive for CD3 & CD4  
970 as shown in figure 5A. All cells were sorted in a MoFlo Astrios (Beckman Coulter) using  
971 Summit Software (Beckman Coulter).

972

### 973 **Immunohistochemical staining:**

974 Human lung tissue containing large airways were collected from archival formalin-fixed  
975 paraffin-embedded (FFPE) blocks (n=10, 6 smokers and 4 non-smokers). Serial sections  
976 (~4 µm) were cut for immunohistochemistry (IHC) and immunofluorescent (IF) staining.

977 Serial sections from FFPE lung tissue were stained for using standard protocols, with  
978 antibodies specified in the figures. Briefly, serial sections were deparaffinized in xylene,  
979 rehydrated and immersed in 10 mM sodium citrate buffer (pH 6.0). Antigen retrieval was  
980 performed by boiling the sections in a pressure cooker at 120°C for 20 min.

981 IHC and IF staining was performed as described previously<sup>49,50</sup>. For the IHC staining cells  
982 were stained with a primary antibody (see below for Ab details) and visualized with  
983 diaminobenzidine (DAB, Sigma) solution. For the IF staining, cells were stained with primary  
984 antibody. Secondary antibodies conjugated to fluorophores (donkey anti rabbit-488, donkey  
985 anti mouse-555) were used at a dilution of 1:100. DAPI, dissolved in Dako Fluorescence  
986 Mounting Medium (Dako S3023) at a dilution of 1:1000, was used as a nuclear stain.

987

988

### 989 **Antibody list:**

990

Antibody	Fluorochrome	Clone	Supplier	Catalog
CD45	BB515	HI30	BD biosciences	564585
CD3	PerCP Cy5.5	SP34-2	BD biosciences	552852

CD4	APC Cy7	RPA-T4	BD biosciences	557871
FOXI1	unlabelled	2B8	LSBio	LS-C336930
CFTR	unlabelled	polyclonal	Human atlas	HPA021939
Synaptophysin	unlabelled	SP11	Ventana Medical Systems	790-4407
MUC5AC	unlabelled	45m1	Abcam	ab3649
KRT5	unlabelled	EP1601Y/LL002	Ventana Medical Systems	760-4939
$\alpha$ -Tubulin	unlabelled	DM1A	Sigma/MERCK	T9026-100UL
Donkey anti rabbit-488	AF 488	Polyclonal	Thermo Scientific Fisher	# A-21206
Donkey anti mouse-555	AF 555	Polyclonal	Thermo Scientific Fisher	# A-31570
DAPI	nuclear stain	n/a	Thermo Scientific Fisher	# D3571

991

992

### Chromium 10x Genomics library and sequencing

993

*Airway biopsy:* Single cell suspensions were manually counted using a haemocytometer and concentration adjusted to a minimum of 300 cells/ul. Cells were loaded according to standard protocol of the Chromium single cell 3' kit in order to capture between 2000-5000 cells/chip position. All the following steps were performed according to the standard protocol. Initially, we used one lane of an Illumina HiSeq 4000 per 10x Genomics chip position. Additional sequencing was performed in order to obtain coverage of at least mean coverage of 100.000 reads/cell.

994

995

996

997

998

999

*Lung transplant:* Single cell suspensions were manually counted using a haemocytometer and concentration adjusted to 1000 cells/ul. Cells were loaded according to standard protocol of the Chromium single cell 3' kit in order to capture between 2000-5000 cells/chip position. All the following steps were performed according to the standard manufacturer protocol. Initially, we used one lane of an Illumina HiSeq 4000 per 10x Genomics chip position. Additional sequencing was performed in order to obtain coverage of at least mean coverage of 100.000 reads/cell.

1000

1001

1002

1003

1004

1005

1006

1007

### SmartSeq 2 library preparation and sequencing

1008

Library preparation was performed with minor modifications from the published SmartSeq2 protocol<sup>51</sup>. In short, single cells were flow sorted onto individual wells of 96 or 384 wells containing 4ul (96 wells) or 1ul (384 wells) of lysis buffer (0.3% triton plus DNTPs and OligoDT). After sorting, plates were frozen and stored at -80 until further processing. RT, PCR (25 cycles) and nextera library preparation performed as described in <sup>51</sup>.

1009

1010

1011

1012

1013

1014

### Dropseq library preparation and sequencing

1015

Drop-seq experiments were performed largely as described previously<sup>7</sup> with few adaptations during the single cell library preparation. Briefly, using a microfluidic polydimethylsiloxane (PDMS) device (Nanoshift), single cells (100/ $\mu$ l) from the lung cell suspension were co-encapsulated in droplets with barcoded beads (120/ $\mu$ l, purchased from ChemGenes

1016

1017

1018

1019

1020 Corporation, Wilmington, MA) at rates of 4000  $\mu$ l/hr. Droplet emulsions were collected for 15  
1021 min/each prior to droplet breakage by perfluorooctanol (Sigma-Aldrich). After breakage,  
1022 beads were harvested and the hybridized mRNA transcripts reverse transcribed (Maxima  
1023 RT, Thermo Fisher). Unused primers were removed by the addition of exonuclease I (New  
1024 England Biolabs), following which beads were washed, counted, and aliquoted for pre-  
1025 amplification (2000 beads/reaction, equals  $\sim$ 100 cells/reaction) with 12 PCR cycles (primers,  
1026 chemistry, and cycle conditions identical to those previously described. PCR products were  
1027 pooled and purified twice by 0.6x clean-up beads (CleanNA). Prior to tagmentation, cDNA  
1028 samples were loaded on a DNA High Sensitivity Chip on the 2100 Bioanalyzer (Agilent) to  
1029 ensure transcript integrity, purity, and amount. For each sample, 1 ng of pre-amplified cDNA  
1030 from an estimated 1000 cells was tagmented by Nextera XT (Illumina) with a custom P5  
1031 primer (Integrated DNA Technologies). Single cell libraries were sequenced in a 100 bp  
1032 paired-end run on the Illumina HiSeq4000 using 0.2 nM denatured sample and 5% PhiX  
1033 spike-in. For priming of read 1, 0.5  $\mu$ M Read1CustSeqB (primer sequence:  
1034 GCCTGTCCGCGGAAGCAGTGGTATCAACGCAGAGTAC) was used.  
1035

### 1036 **Bulk Transcriptome**

1037 Biopsies were fresh frozen in liquid nitrogen and stored in -80. RNA was extracted after a  
1038 few weeks using a combination of Trizol & the RNeasy MinElute Clean Up kit from Qiagen.  
1039 RNA was prepared from sequencing using the TruSeq RNA Library Prep Kit v2. Samples  
1040 were then sequenced in a HiSeq 4000.  
1041

### 1042 **Single-cell RNA sequencing data alignment**

1043 For SmartSeq2 raw sequencing data, paired-end reads were mapped to the Human genome  
1044 (GRCh38) using GSNAP with default parameters<sup>52</sup>. Then, uniquely mapped reads were  
1045 counted using htseq-count (<http://www-huber.embl.de/users/anders/HTSeq/>). Low-quality  
1046 cells were filtered out using the outlier detection algorithm in R Scater package based on a  
1047 cut-off of  $2 * MAD$  (median-absolute-deviation).  
1048

1049 10X Genomics raw sequencing data was processed using CellRanger software version  
1050 2.0.2 and the 10X human genome GRCh38 1.2.0 release as the reference.

1051 The Dropseq core computational pipeline was used for processing next generation  
1052 sequencing reads of the Dropseq scRNA-seq data, as previously described<sup>7</sup>. Briefly, STAR  
1053 (version 2.5.2a) was used for mapping<sup>53</sup>. Reads were aligned to the human reference  
1054 genome hg19 (provided by Dropseq group, GSE63269).  
1055

### 1056 **Bulk transcriptome computational analysis**

1057 The bulk samples were aligned using STAR 2.5.1b, using the STAR index from the GRCh38  
1058 reference that was used when mapping 10X data, and quantified using HTSeq. The data  
1059 was then processed using the Seurat-inspired workflow within Scanpy, adding a number of  
1060 "pseudo-bulks" obtained by taking 10X data from donors matching the bulk samples and  
1061 summing expression across all cells.  
1062

### 1063 **Data QC**

1064 *General strategy for 10x datasets:* Optimal tissue dissociation conditions are cell-type  
1065 dependent, resulting in a certain degree of cell lysis when working with a mixed tissue  
1066 sample. This results in substantial background levels of ambient RNA in the single-cell  
1067 suspension that vary with cell type composition, so we applied SoupX for background  
1068 correction (see below). We analysed each donor sample separately and excluded cells with  
1069 a number of genes higher than the median+2SDs for that donor. We further excluded cell  
1070 with high number of UMIs and high percentage of mitochondrial reads (see below).



1071 In parallel, we used scrublet (see below) to infer the number of the doublets in the dataset  
1072 before applying the filters previously described and excluded any remaining cells predicted  
1073 to be doublets that were still present in the dataset. We normalised and scaled our data (see  
1074 below), performed clustering (see below) and identified and subset the data into epithelial  
1075 and non-epithelial cell groups (as shown in supplementary figures 1 and 6). After separation  
1076 between epithelial and non-epithelial, we clustered the cells and performed curated doublet  
1077 removal (see below) based on known lineage restricted markers.

1078  
1079 *General strategy for Dropseq data:* We normalised and scaled the data, then performed  
1080 filtering based on the number of genes and percentage of mitochondrial reads.

1081  
1082 *General strategy smartseq2 data:* We normalised and scaled the data, then performed  
1083 filtering based on the number of genes and percentage of mitochondrial reads. In order to  
1084 avoid potential batch effects from the lung digestion protocol, we corrected the gene  
1085 expression of the CD4 SmartSeq2 dataset using a small subset of genes the expression of  
1086 which has been recently shown to be highly responsive to enzymatic digestion<sup>54</sup> : FOS,  
1087 ZFP36, JUN, FOSB, HSPA1A, JUNB, EGR1, UBC.

### 1088 1089 **Ambient RNA correction (SoupX)**

1090 Different batches can be affected by different levels of ambient RNA. To take this into  
1091 account, we used the recently developed SoupX method<sup>55</sup>. Briefly, ambient RNA expression  
1092 is estimated from the empty droplet pool (10 UMI or less). Expression of these genes in each  
1093 cell is then calculated and compared to their proportion in the ambient RNA profile.  
1094 Transcripts with a bimodal profile (i.e. that characterize specific groups of cells but are also  
1095 highly abundant in empty droplets) are then grouped based on their function. The  
1096 contamination fraction derived from the expression of these genes is then used to calculate  
1097 the fraction of each droplet's expression corresponding to the actual cell. Finally, this fraction  
1098 and the ambient profiles are subtracted from the real expression values.

### 1099 1100 **UMI and number of genes filtering**

1101 *10x data (After SoupX correction):*  
1102 nUMI: minimum 1000/ maximum 60000.  
1103 percent.mito, minimum 0 / maximum= 3%

1104 *SmartSeq2 data:*  
1105 nGene : minimum 1000 / maximum 4000.  
1106 percent.mito, minimum 0 / maximum= 15%

1107 *Dropseq data:*  
1108 nGene: minimum 200/ maximum 4000.  
1109 percent.mito, minimum 0 / maximum= 20%

### 1110 1111 **Scrublet**

1112 We used Scrublet (Wolock et al, BioRxiv, <https://doi.org/10.1101/357368>) for unbiased  
1113 computational doublet inference. Doublets were identified in each 10X sample individually  
1114 using scrublet, setting the expected doublet rate to 0.03 and keeping all other parameters  
1115 at their default values. Cells were excluded when they had a score higher than 0.1 for upper  
1116 and lower airway samples or higher than 0.05 for parenchyma samples.

### 1117 1118 **Normalisation and scaling**

1119 Downstream analyses including, normalisation, scaling, clustering of cells and identifying  
1120 cluster marker genes were performed using the R software package Seurat<sup>48</sup> version 2.1  
1121 (<https://github.com/satijalab/seurat>).



1122 Samples were log normalised and scaled for the number of genes, number of UMIs and  
1123 percentage of mitochondrial reads. The epithelial biopsy dataset comparing healthy and  
1124 asthma was also scaled for XIST expression, as we observed some gender specific clusters  
1125 of cells that shared lineage markers with the other observed clusters.

1126

### 1127 **Curated doublet removal**

1128 We combined literature knowledge about cell lineages with over clustering to identify  
1129 clusters enriched in potential doublets. The strategy for each dataset is shown below:

1130

1131 *Lung atlas epithelial dataset* (Figure 1 and associated extended data figures): We removed  
1132 cells with expression level higher than 0.5 for any of the following markers: PTPRC  
1133 (immune),FCER1G (immune), PDGFRA (fibroblast) or PECAM1 (endothelial).

1134

1135 *Lung atlas non-epithelial dataset* (Figure 2 and associated extended data figures): We  
1136 removed cells with expression level higher than 0.5 for any of the following markers: EPCAM  
1137 (epithelial),KRT5 (basal), “FOXJ1”(ciliated) or MUC5AC (secretory). We then performed first  
1138 clustering round (7 PCs, resolution 2) and excluded clusters that expressed combinations  
1139 of the following lineage specific markers: MARCO(macrophage), CCL21 (lymphatic  
1140 endothelial), TPSB2 (mast cell) or CD3D(T cell). We performed a second clustering round  
1141 and exclude a cluster formed by cells from one donor that had low expression TPSB2, while  
1142 lacking markers for all other immune lineages.

1143

1144 *Asthma biopsy epithelial cells* (Figure 3 and associated extended data figures): due to the  
1145 smaller number of cells, we only performed cluster-based doublet exclusion, without cell  
1146 filtering. We performed one round of clustering and removed one clusters with high  
1147 expression of PECAM1 (endothelial marker).

1148

1149 *Asthma biopsy non-epithelial cells* (Figure 4 and associated extended data figures): we  
1150 performed three rounds of clustering where we excluded clusters with high levels of EPCAM  
1151 or KRT5 expressed in much higher levels than immune lineage markers.

1152

### 1153 **Dimensionality reduction**

1154 We performed PCA dimensionality reduction with the highly variable genes as input. We  
1155 then used the PCs to calculate t-Distributed Stochastic Neighbour Embedding (**t-SNE**) for  
1156 each dataset, using a perplexity value of 50.

1157

### 1158 **Data clustering**

1159 We used the function “FindClusters” from Seurat. In brief, this method uses a shared nearest  
1160 neighbour (SNN) modularity optimization-based clustering algorithm to identify clusters of  
1161 cells based on their PCs. Before constructing the SNN graph, this function calculates k-  
1162 nearest neighbours (we used k=30) and then it constructs the SNN graph. The number of  
1163 PCs used for each clustering round was dataset dependent and they were estimated by the  
1164 elbow of a PCA scree plot, in combination to manual exploration of the top genes from each  
1165 PC.

1166

### 1167 **DE analysis**

1168 We used a Wilcoxon rank sum test to identify differentially expressed genes in all the  
1169 comparisons here discussed.

1170

### 1171 **MatchScore**

1172 We used MatchScore<sup>8</sup> to quantify the overlap of cell type marker signatures between  
1173 experiments, which is based on the Jaccard index. Only marker genes with adjusted p-value  
1174 < 0.1 and average log fold change > 1 were considered.

1175

### 1176 **CellPhoneDB**

1177 We developed a manually curated repository of ligands, receptors and their interactions  
1178 called CellPhoneDB ([www.cellphonedb.org](http://www.cellphonedb.org); Vento-Tormo, Efremova et al., *Nature*, 2018),  
1179 integrated with a statistical framework for predicting cell-cell communication networks from  
1180 single cell transcriptome data. Briefly, the method infers potential receptor-ligand  
1181 interactions based on expression of a receptor by one cell type and a ligand by another cell  
1182 type. Only receptors and ligands expressed in more than 30% of the cells in the specific  
1183 cluster were considered. In order to identify the most relevant interactions between cell  
1184 types, the method prioritizes ligand-receptor interactions that have cell type-specific  
1185 expression. To this end, pairwise cluster-cluster interaction analysis are performed by  
1186 randomly permuting the cluster labels of each cell 1000 times. For each permutation, the  
1187 total mean of the average receptor expression level of a cluster and the average ligand  
1188 expression level of the interacting cluster is calculated, and a null distribution is derived for  
1189 each receptor-ligand pair in each cluster-cluster interaction. An empirical *p*-value is  
1190 calculated from the proportion of the means which are "as or more extreme" than the actual  
1191 mean. For the multi-subunit heteromeric complexes, the member of the complex with the  
1192 minimum average expression is used for calculating the mean.

1193 Network visualization was done using Cytoscape (version 3.5.1). All the interaction pairs  
1194 with collagens were removed from the analysis. The networks layout was set to force-  
1195 directed layout.

1196

### 1197 **Trajectory analysis**

1198 Trajectory analysis was performed using Monocle version 2.2.0<sup>23</sup>. We ordered the cells onto  
1199 a pseudotime trajectory based on the union of highly variable genes obtained from all cells,  
1200 as well as those from only healthy or asthmatic donors.

1201

### 1202 **Supervised analyses using GWAS genes**

1203 Asthma-associated GWAS gene list was collected using the GWAS Catalog of EMBL-EBI  
1204 searching for the term asthma (<https://www.ebi.ac.uk/gwas/>). The list was downloaded on  
1205 8th of February 2018. We took the genes that are in the top 50 hits of our single-cell DE  
1206 marker list (either epithelial or non-epithelial) and asthma-associated GWAS list (the  
1207 "matched" gene list). We then hierarchically clustered the expression matrix of the matched  
1208 gene list along its rows (genes) and columns (single cells) and represented this as a  
1209 heatmap.

1210

### 1211 **Neuroendocrine cell identification**

1212 Neuroendocrine cells were identified by the expression of CHGA. Any cell expressing any  
1213 amount of CHGA was classified as a neuroendocrine cell.

1214

### 1215 **OMIM search for lung diseases**

1216 We searched the clinical synopses with known molecular basis in the Online Mendelian  
1217 Inheritance in Man (OMIM) database<sup>®</sup> for the following terms: 'pulm\*' or 'bronchi\*' or 'alveol\*'  
1218 or 'surfactant' and retrieved 337 entries. These terms were chosen to minimise the return of  
1219 genetic conditions causing respiratory insufficiency as a consequence of neuromuscular  
1220 dysfunction, skeletal dysplasia (small rib cage) or lung segmentation defects arising in early  
1221 embryogenesis. These 337 entries were then manually curated to identify those conditions  
1222 with features affecting the bronchial tree, alveoli, lung parenchyma and pulmonary  
1223 vasculature. On manual review, entries containing terms such as 'alveolar ridge' of the jaw

1224 and 'pulmonary valve stenosis' and 'pulmonary embolism', but no terms related to primary  
1225 pulmonary disorders, were excluded from further consideration. Syndromes caused by  
1226 chromosomal disorder or contiguous gene deletion were excluded.

1227

### 1228 **Statistical methods**

1229 For 10x samples comparing healthy versus asthma, we used Fisher's exact test corrected  
1230 for multiple testing with Bonferroni method. Normalised CD4 cluster proportions were  
1231 analysed via paired t-tests corrected for multiple testing with Holm-Sidak method.

1232

1233

